

ABSTRACT

POLLEN, AUDRIANNA FITZGERALD. The Sedimentary Record of Past Earthquakes Identified in Holocene Sediments of Lake Crescent, Washington. (Under the direction of Dr. Elana L. Leithold).

This study aims to resolve the influence of large earthquakes on sediment accumulation in Lake Crescent, Washington over the past ~8500 years. Lake Crescent is located on the north Olympic Peninsula, west of the Cascade volcanic arc and above the Cascadia subduction zone. Identifying the event deposits produced by mass movements in the lake and their possible correlation with earthquakes is important to the understanding of past and future natural hazards in the area. Sediment cores extracted from Lake Crescent include four types of event layers: megaturbidite, turbidite, slump, and slide deposits. Four widely distributed >1.3 m thick 'megaturbidite' deposits are characterized by three distinct units: a fining upward, coarse-grained basal layer that is overlain by a massive silty unit, which is topped by a faintly laminated to massive clay cap. Previous research indicates these types of layers may form when subaerial landslides entering lakes trigger lake tsunamis and subsequent seiches. Large landslides have been mapped around and within Lake Crescent. Offset lake sediments imaged in seismic reflection profiles furthermore provide evidence that these landslides and tsunami/seiche events were related to ruptures of faults that run directly beneath the lake, which would have generated strong ground shaking. Radiocarbon analyses indicate that the megaturbidites record four such catastrophic events that occurred around 2959, 4015, 5736, and 7097 cal yr BP.

Nineteen 2- to 33-cm-thick turbidite layers are also present in the lake record. The volume of sediment in each of these turbidite layers is greater than would be expected from episodic flooding of streams discharging to the lake. This suggests that these turbidites instead record seismically triggered remobilization of sediments stored on the margins and slopes within the lake. Finally, the slump and slide deposits are inferred to record mass wasting on subaqueous and subaerial slopes surrounding the lake. The Lake Crescent event record is compared to previously dated deposits from Effingham and Saanich Inlets, Canada and the deep sea floor, all inferred to record ruptures of the Cascadia subduction interface. Thirteen of the event layers in Lake Crescent were found to temporally overlap with one or more of the comparison paleoseismic records, supporting the hypothesis that they also record regional earthquakes. The recurrence interval between

megaturbidites is ~1100-1700 years with the last event occurring ~3000 years ago, while the time between turbidites is ~320 years. Evidence for earthquake-triggered mass wasting in Lake Crescent suggests that that the lake is at risk for similar, perhaps devastating, events in the future.

© Copyright 2016 by Audrianna Fitzgerald Pollen

All Rights Reserved

The Sedimentary Record of Past Earthquakes Identified in Holocene Sediments of Lake Crescent,
Washington

by
Audrianna Fitzgerald Pollen

A thesis submitted to the Graduate Faculty of
North Carolina State University
in partial fulfillment of the
requirements for the degree of
Master of Science

Marine, Earth, and Atmospheric Science

Raleigh, North Carolina

2016

APPROVED BY:

Dr. Elana L. Leithold
Committee Chair

Dr. Karl W. Wegmann

Dr. Delwayne R. Bohnenstiehl

DEDICATION

To my father for his ongoing support and for encouraging my childhood rock collection, which mainly boasted an array of pretty pieces of gravel. To my step-father for his unending support of my dreams. To my mother, my best friend, for her endless support, encouragement, and love; without her many cross country phone calls, long car rides to and from the airport, and words of inspiration, I would not be where I am today. To my friends who became family and every teacher, professor, and mentor who believed in me. Also to green tea, without which I never would have made it to this point.

Crom A Boo (Crom to Victory)

BIOGRAPHY

I grew up in in the mountains of California, attended Occidental College in the city of Los Angeles, studied abroad at the University of Otago in Dunedin, New Zealand, and pursued my Master's degree at North Carolina State University in Raleigh, North Carolina. Along the way I laughed, cried, sweat, bled, and somehow ended up here.

ACKNOWLEDGMENTS

I would like to thank my adviser, Dr. Lonnie Leithold for her unending support and patience over the past two years, at times I wasn't sure I would make it, but with her help, I did it! I also would like to express my gratitude to my committee members, Dr. Karl Wegmann and Dr. DelWayne Bohnenstiehl, thank you for pushing me to think things through and spending the time to help me produce my best work. In addition, this project would not have been possible without the amazing team from LacCore, Kristina Brady, Anders Noren, Mark Shapley, and Ryan O'Grady.

Financial support for this project was provided by a U.S. Geological Survey – National Earthquake Hazards Reduction Program Grant (Award # G15AP00091). Research within Olympic National Park was conducted under Special Use Permit # OLYM-366.

TABLE OF CONTENTS

LIST OF TABLES	vii
LIST OF FIGURES	viii
1. INTRODUCTION	1
2. GEOLOGIC SETTING	3
2.1 Tectonic Setting	4
2.2 Lake Setting	7
3. METHODS	10
3.1 Geophysical Data Collection	10
3.2 Sediment Core Collection	11
3.3 Sediment Core Processing	12
3.4 Particle Size Analysis	13
3.5 Radiocarbon Sample Processing	14
3.6 Age Models	15
4. RESULTS	16
4.1 Sedimentary Deposits	16
4.2 Event-Free Depth	25
4.3 Age Models and Accumulation Rates	26
5. EVENT LAYER HISTORY AND CORE STRATIGRAPHY	29
5.1 Megaturbidites	29
5.2 Turbidites	32
5.3 Landslide and Slump Deposits	38
6. DISCUSSION AND INTERPRETATION	42
7. CONCLUSIONS	51
7.1 Summary	51
7.2 Seismic Hazards	52
REFERENCES	53

APPENDICES.....	60
Appendix A. Major tributaries in the Lake Crescent watershed	61
Appendix B. Accumulation rate calculations for sediment cores with multiple radiocarbon ages	62
Appendix C. Event layers present in the sediment record and their respective thicknesses and ages	63
Appendix D. EL2 deposits volume and annual average sediment yield compared to the Hoh River.....	66
Appendix E. Amount of record missing from top of sediment cores calculations	68

LIST OF TABLES

Table 1. Event free length compared to core depth for the 14 collected Kullenberg cores	25
Table 2. Lake Crescent Radiocarbon Dates	26
Table 3. Description of the nineteen LCT (Lake Crescent Turbidite) event layers	36
Table 4. Lake Crescent EL1 and EL2 layers correlated to the seismic event records of Effingham Inlet, Saanich Inlet, and the combined offshore turbidite record.....	49

LIST OF FIGURES

Figure 1. Location of Lake Crescent and surrounding features	3
Figure 2. Simplified geologic map of the Lake Crescent area.....	5
Figure 3. Sadie Creek fault scarp trace visible in the bare earth LiDAR data	6
Figure 4. Preliminary bathymetric map of Lake Crescent	9
Figure 5. Kullenberg core collection sites on bathymetric map of Lake Crescent and topographic map of surrounding region.....	12
Figure 6. Median particle size (red) and magnetic susceptibility (black) for the thick event deposit present in core 2C-1K (depth 97-245 cm).	14
Figure 7a. Event Layers correlated across the northern basin of Lake Crescent.	18
Figure 7b. Continued Event Layers correlated across the northern basin of Lake Crescent.....	19
Figure 7c. Event layers correlated through the broad channel connecting the northern and southern basins in Lake Crescent	20
Figure 7d. Event layers correlated through the southern basin of Lake Crescent	21
Figure 7e. Continued event layers correlated through the southern basin of Lake Crescent	22
Figure 8. CHIRP seismic profile image obtained from the northern basin	24
Figure 9. Age models interpolated from the Bayesian age modeling program Bacon for cores 4A-1K, 6A-1K, and 7C-1K	28
Figure 10. Five core images depicting the uppermost megaturbidite (EL1-A) deposit with a description of the typical megaturbidite facies.....	30
Figure 11. Core images and descriptions of landslide and slump deposits	41
Figure 12. EL1 and EL2 event deposits correlated across Lake Crescent	43
Figure 13. EL2 layers correlated (dashed black lines) above the first megaturbidite deposit (EL1-A) that is indicated by red symbology	44
Figure 14. Offset sediment layers in a CHIRP seismic profile image.....	46
Figure 15. Age of Lake Crescent EL1 and LCT deposits compared to the seismic records of Effingham Inlet, Saanich Inlet, and the combined offshore turbidite record.....	48

1. INTRODUCTION

Examining the past history of natural hazard events is paramount to predicting their future impact. Lake Crescent, located near population, transport, utility, and industry centers, is in a region that would be severely impacted by a large earthquake or landslide event. Geologic events such as landslides and earthquakes have been observed in western Washington causing damage to property and lives. Of particular note, in 1965 a magnitude 6.5 earthquake shook the Puget Sound region causing \$12.5 million in property damage and killing seven people while in 2001 the Nisqually earthquake caused over \$2 billion in estimated total economic losses in Washington State and one death (Stover & Coffman, 1993; Meszaros & Fiegener, 2002). Determining the paleoseismic history of the region will help define hazards associated with future earthquake events.

Lakes often contain important sedimentary archives of past earthquakes, including information about much longer time periods than is available from historical records (Karlin & Abella, 1992; Inouchi et al., 1996; Hilbe & Anselmetti, 2014; Moernaut et al., 2014; Van Daele et al., 2015, Kremer et al., 2015, among others). Archaeological evidence and native oral traditions reveal that Native American villages along the coasts of Washington and southern British Columbia were abandoned from the effects of rupture along the northern Cascadia subduction zone (Hutchinson & McMillan, 1997). However, these oral traditions can prove difficult to precisely date and may be lost to time. Lake Crescent is in an ideal location to preserve sedimentary archives of past regional events. It is deep (~190 meters) and oligotrophic so sediments are minimally disturbed by bioturbation. Events such as landslides, earthquakes, and floods can leave distinctive sedimentary deposits attesting to within-lake mass movements contained within an overall package of background sedimentation in the lake. Examining these deposits can elucidate the geologic history of the lake.

Distinct sedimentary deposits have been linked to catastrophic events such as landslides and earthquakes in lake records from many locations, including the earthquake-prone regions of Lake Lucerne, Switzerland (Hilbe & Anselmetti, 2014), central Chile (Moernaut et al., 2014; Van Daele et al., 2015), Lake Biwa, Japan (Inouchi et al., 1996), and Lake Washington, located just east of Seattle, Washington (Karlin & Abella, 1992). Earthquakes were found to mobilize sediment and trigger mass wasting events into lakes leaving an identifiable paleoseismic signature. Notably, turbidite deposits

linked to seismic events were found within each lake in the aforementioned locations and their presence has been used to help construct the regional paleoseismic event histories.

Large, prehistoric earthquakes shook the Olympic Peninsula many times in the past. Research involving submerged forest dendrochronology, coastal subsidence, tsunami deposits, and offshore turbidites indicates that the Cascadia subduction zone has ruptured many times in the past generating great earthquakes of magnitude 8.0-9.0 (e.g. Atwater, 1987; Atwater & Hemphill-Haley, 1997; Goldfinger et al., 2012). Furthermore, upper crustal faults running near and directly under Lake Crescent may have generated earthquakes with epicenters very near the lake (Nelson et al., 2007). Several landslide scarps are present on the steep slopes surrounding Lake Crescent which may have been seismically triggered and deposited material directly into the lake. Minimal delivery of fluvial sediments to Lake Crescent lends credence to the proposed idea that sedimentary event deposits preserved in the lake were triggered by subaqueous or subaerial mass wasting, rather than episodic strong flooding events. Attribution of such deposits to past regional earthquakes, moreover, can be strengthened by comparison to inferred seismically induced deposits in other nearby locations. This study uses the lacustrine sedimentary archive of Lake Crescent to elucidate the Holocene paleoseismic history of the north-central Olympic Peninsula for the purpose of improving our understanding and prediction of future geologic hazards in western Washington State.

2. GEOLOGIC SETTING

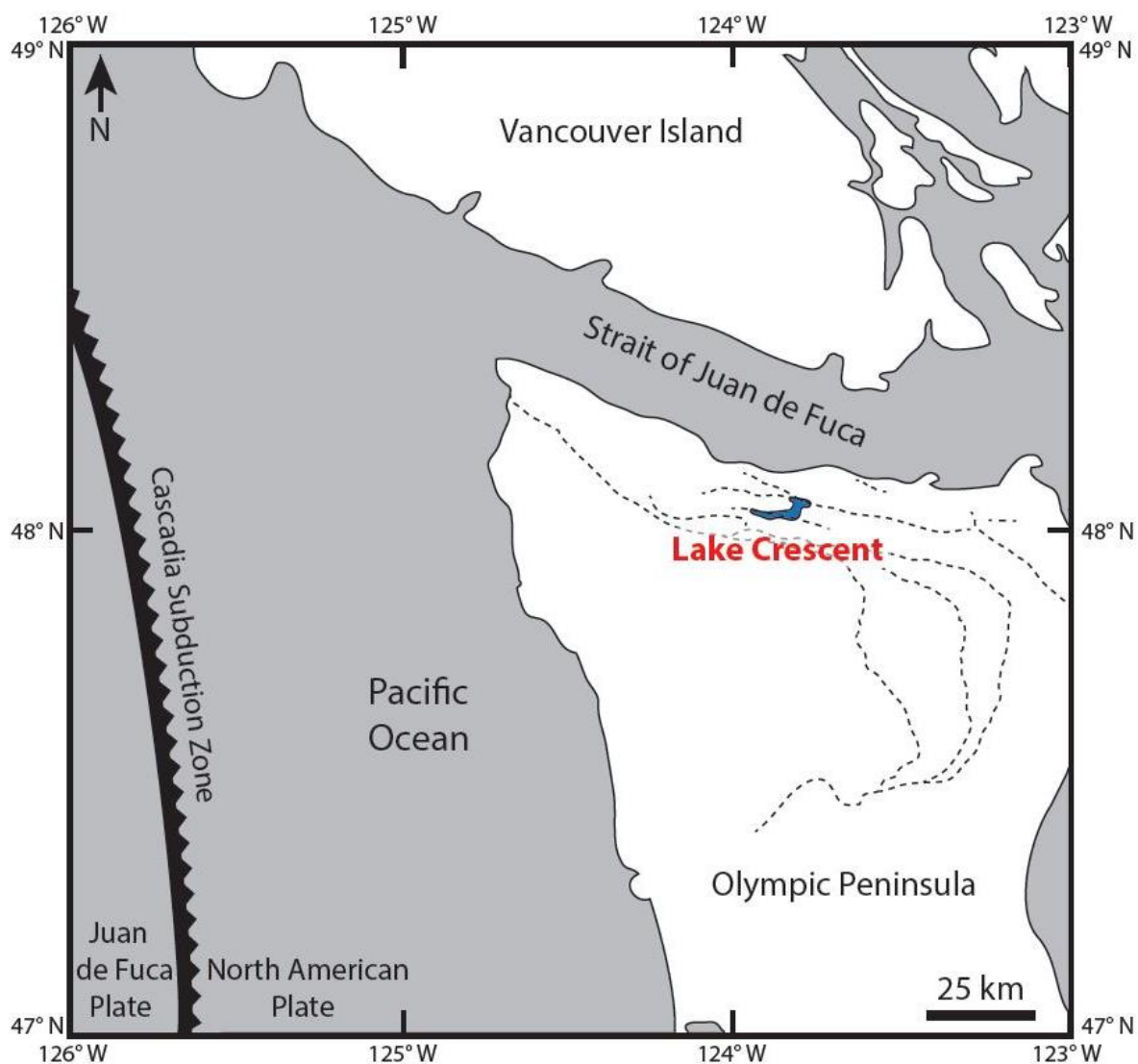


Figure 1. Location of Lake Crescent and surrounding features. Upper crustal faults indicated by dashed black lines.

The 20.8 km² Lake Crescent is located on the northern end of the Olympic Peninsula of Washington State just within the boundary of Olympic National Park. The Strait of Juan de Fuca lies to the north, separating the Olympic Peninsula from Vancouver Island, British Columbia (Fig. 1). The Olympic Mountains lie mainly south and southwest of Lake Crescent reaching a height of 2,427 m at the summit of Mount Olympus. The Cascadia subduction zone, which lies offshore to the west of the Olympic Peninsula exerts an influence on the geology of the entire region. The Cascadia subduction margin extends 1,100 km from Vancouver Island in southern British Columbia to Cape Mendocino off

the coast of northern California. This plate boundary has produced extremely large and dangerous (magnitude >8.0) earthquakes during stress release associated with subduction of the Juan de Fuca plate beneath North America (e.g. Wells et al., 1998).

2.1 Tectonic Setting

The Olympic Peninsula is a geologically active region under tectonic stress from the northeastward oblique subduction of the Juan de Fuca plate under the North American plate. This relative plate motion is responsible for the complex, seismically active Cascadia convergent margin (Wells et al., 1998). The most recent and well-constrained subduction zone earthquake occurred in 1700 C.E., generating a magnitude 9.0 earthquake that ruptured at least 900 km of the plate boundary (Yamaguchi et al., 1997). This predates written historical archives in North America, which is the reason for the fairly recent discovery that Cascadia produces large magnitude earthquakes (Heaton & Hartzell, 1987). Several studies found geologic records of onshore tsunami deposits and co-seismic coastal subsidence that would likely only be generated during a large offshore earthquake (Atwater, 1987; Atwater & Yamaguchi 1991; Shennan et al., 1996; Clague, 1997). These data, compiled with the offshore turbidite record collected by Goldfinger et al. (2012) provides strong evidence that the Cascadia subduction zone generates great earthquakes with a recurrence interval of ~500 years. Estimates from Adams (1990) and Goldfinger et al. (2012) indicate a full rupture of the Cascadia plate margin (magnitude ~9.0) has occurred 13 to 14 times in the past ~7,500 years.

The Cascadia forearc is migrating northward and rotating clockwise at up to 2.0°/Ma causing north-south shortening in western Washington (Wells et al., 1998; McCaffrey et al., 2007). GPS data indicate this long term north-south shortening is occurring at a rate of ~3.0 to 3.5 mm/yr which falls off to near zero in British Columbia (Mazzotti et al., 2002). The crustal shortening is mostly accommodated by east-west trending thrust faults in the Puget Sound-Georgia Basin and Olympic Mountain region (Wells et al., 1998; Mazzotti et al., 2002). Evidence for a magnitude 7.0 to 7.5 event on the Seattle fault ~1100 years ago indicates that these faults pose a credible geologic hazard (Atwater & Moore, 1992; ten Brink et al., 2006). However, the potentially damaging consequences of upper-plate earthquakes is less well known than for subduction zone events, due to sparse exposure

of active structures as well as a short historical record and longer recurrence intervals between earthquakes (Wells et al., 1998). Lake Crescent is located in a region that could be affected by earthquakes generated on both nearby crustal faults as well as the offshore megathrust events.

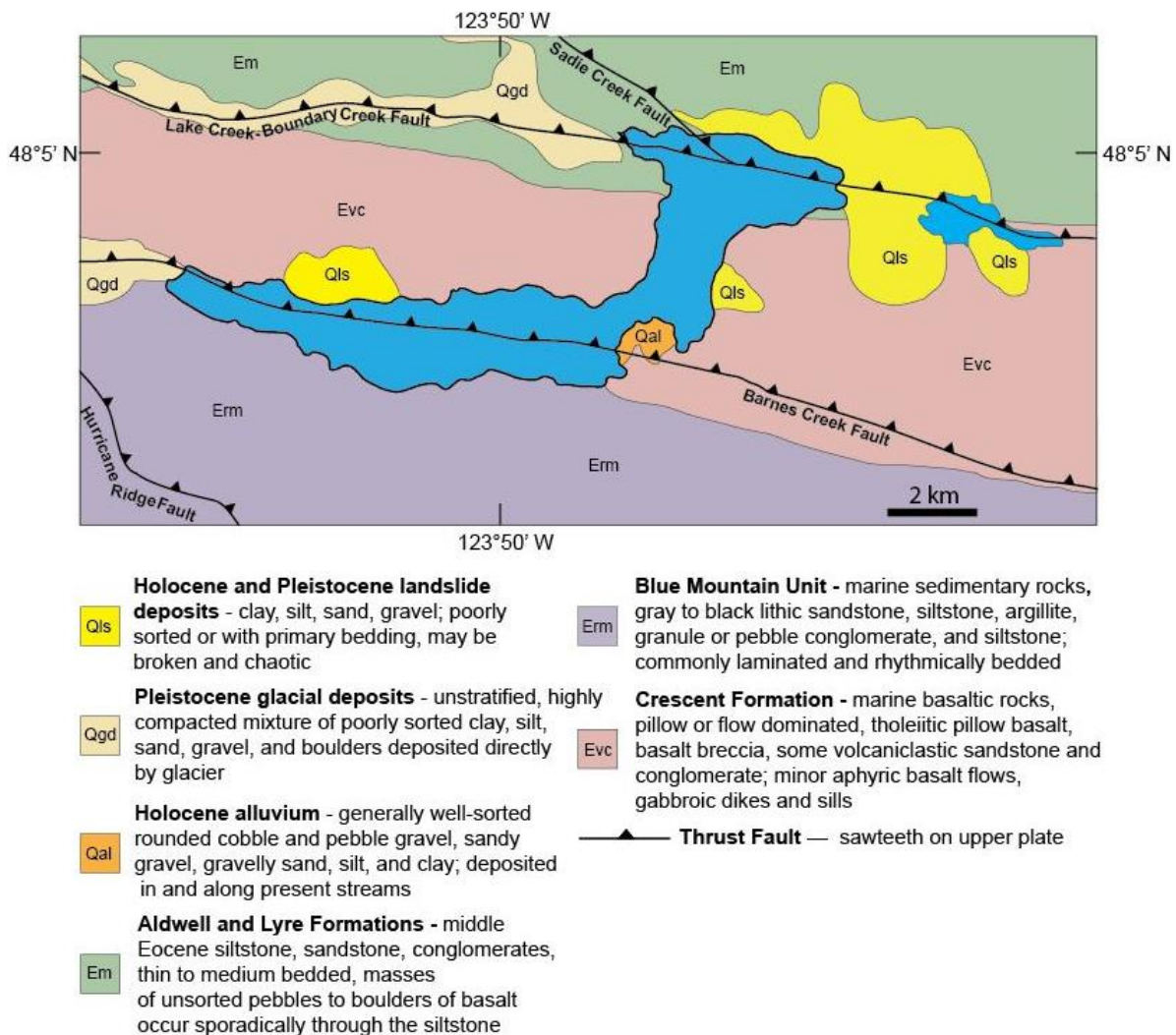


Figure 2. Simplified geologic map of the Lake Crescent area adapted from Schasse (2003). Lake Sutherland lies to the east of the larger Lake Crescent.

Three major, east-west trending, north-dipping faults on the northern edge of the Olympic Mountains are located close to Lake Crescent (Tabor & Cady, 1978; Schasse, 2003; Polenz et al., 2004). The Hurricane Ridge fault lies to the south of Lake Crescent while the Barnes Creek fault appears to run underneath the southern basin of Lake Crescent (Schasse, 2003; Fig. 2). The Lake Creek–Boundary Creek fault and the herein named Sadie Creek fault splay trend underneath the northern basin of the lake. Polenz et al. (2004) observed possible surface lineaments and scarps

suggesting postglacial movement along the Lake Creek–Boundary Creek fault east of Lake Crescent. Trenching of the Lake Creek–Boundary Creek fault south and east of Port Angeles produced evidence of three surface faulting earthquake events in the past ~5000 years in addition to evidence for significant lateral as well as vertical slip during the earthquake events that formed the surface features (Nelson et al., 2007). Further evidence for local fault motion is the 2 to 3 m fault scarp visible in recently obtained LiDAR data along the Sadie Creek fault; offset along the scarp indicates fault motion included components of both vertical and right lateral motion (Puget Sound, 2015; Fig. 3). A lack of movement along these faults in recorded history makes it difficult to determine how these earthquakes impacted Lake Crescent, but ground shaking from a local fault rupture could conceivably trigger a subaerial mass wasting event into Lake Crescent.

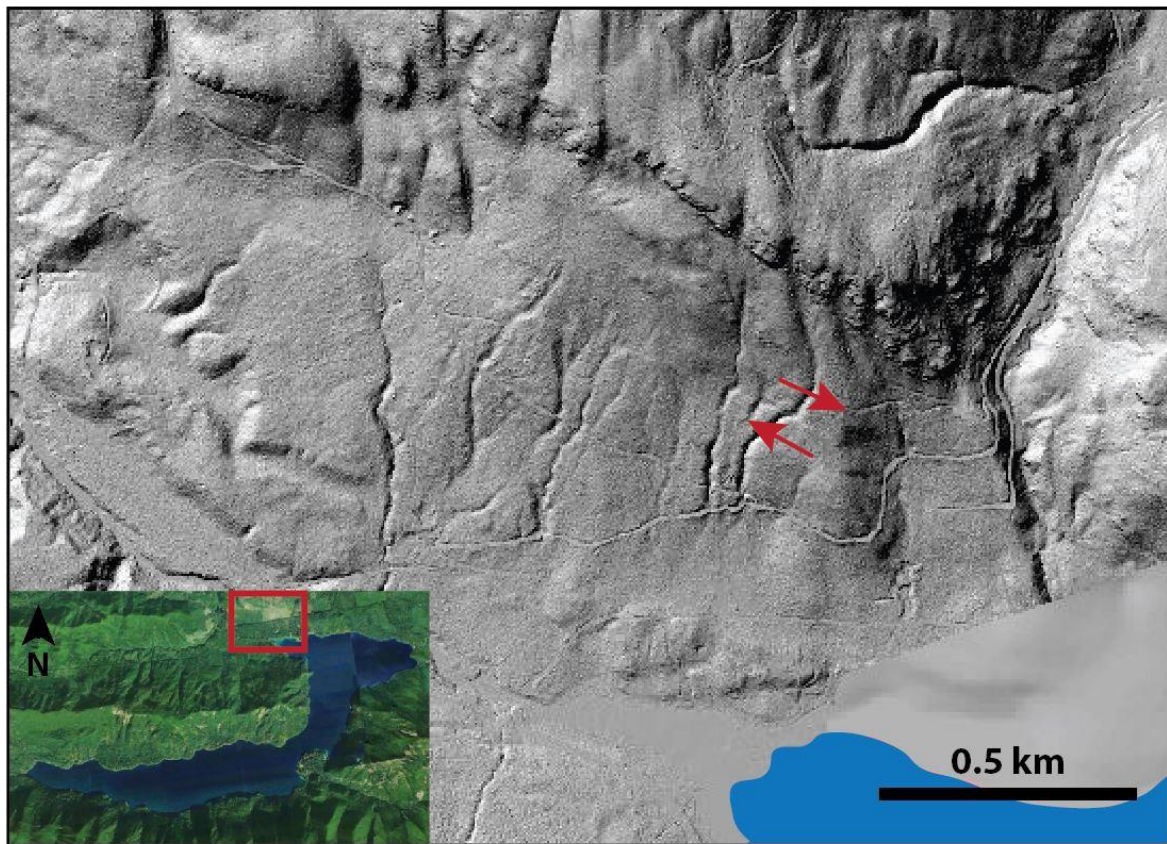


Figure 3. Sadie Creek fault scarp trace visible in the bare earth LiDAR data (Puget Sound, 2015). Right lateral motion marked by red arrows is indicated by the offset drainages.

2.2 Lake Setting

The Lake Crescent basin was formed by repeated scouring and subglacial erosion from the most recent and predecessor advances of the Juan de Fuca lobe of the Cordilleran Ice Sheet. Two elongate basins comprise Lake Crescent, a smaller northern basin and a larger southern basin, connected by a broad channel. The western portion of the southern basin is shallow relative to the rest of the sub-basin and partially isolated from the rest of the lake by landslide deposits (Fig. 4). The far western edge of the southern basin was formed by the recessional moraine of a lobe of the Cordilleran ice sheet at c. 14 to 13 ka (Logan & Schuster, 1991). Subsequent glacial melting formed one large lake in the area, encompassing the modern areas of Lake Crescent and the eastern adjacent Lake Sutherland (Logan & Schuster, 1991). Sometime after the glacial recession a large landslide separated the two lakes, blocking Lake Crescent's egress to the Strait of Juan de Fuca via the Elwha River, and causing the lake level to rise to its modern elevation 25 m above Lake Sutherland (Logan & Schuster, 1991). A submerged tree from the western portion of the southern basin that is rooted in the lake bottom at a water depth of 18 m was cored by U.S. National Park Service divers in the 1990's. The radiocarbon age for the outermost preserved ring of the tree produced an age of ~4340 cal BP, which serves as a limiting maximum age of the landslide event (Wegmann et al., 2014).

The southern basin is flanked by east-west trending, steeply dipping ridges; as much as half of the hillslopes facing the lake exceed a gradient of 30° (Moran et al., 2013). Both lake basins lie between west-northwest trending blocks of mainly marine thrust-faulted rocks. Flanking the southern lakeshore, the early Tertiary Blue Mountain Unit is dominated by thinly-bedded turbidites interstratified with massive sandstone layers with a few massive to finely laminated and rhythmically bedded siltstone beds interspersed throughout (Babcock et al., 1994; Fig. 2). Middle Eocene sedimentary rocks such as thin to medium bedded siltstone, sandstone, and conglomerates comprise the Aldwell and Lyre Formations, surround much of the northern basin (Schasse, 2003; Fig. 2). Bordering the northern edge of the southern basin as well as much of the eastern shoreline is the Crescent Formation, which is predominantly composed of Paleocene-to-Eocene marine basalts and minor associated sedimentary rocks (Schasse, 2003; Fig. 2). Distinct landslide scarps are present on

several of the lake-facing slopes and can be correlated to subaqueous landslide deposits observed in the bathymetry of the lakebed (Fig. 2 & 4).

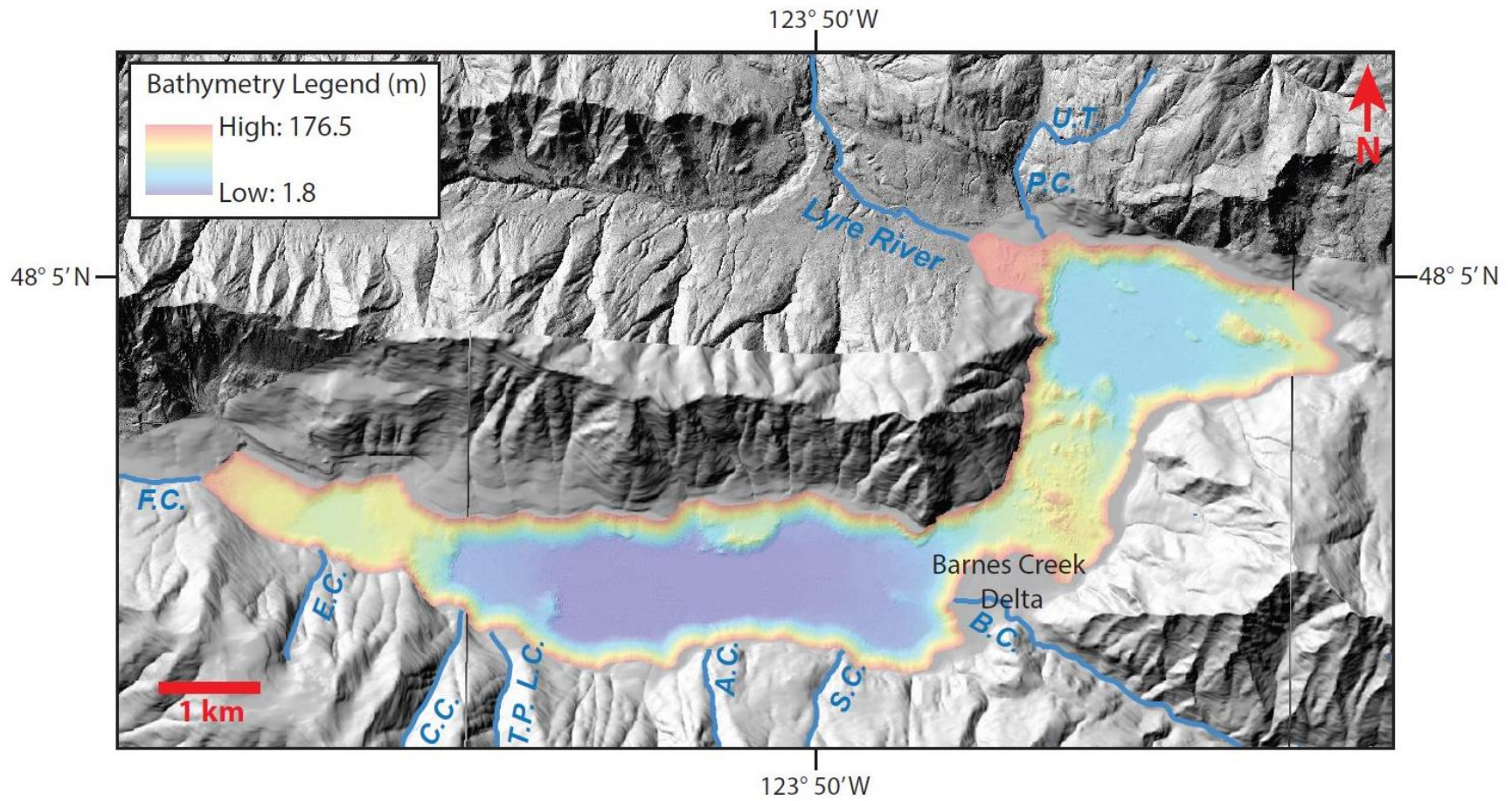


Figure 4. Preliminary bathymetric map of Lake Crescent. Bathymetric map has a grid cell resolution of 3 m and the values are elevations not water depths. Surrounding topography is a 10 m DEM (USGS, 2001) with a higher resolution bare earth floating point LiDAR DEM north of the lake (Puget Sound, 2015). Significant streams and tributaries flowing into Lake Crescent are indicated by their abbreviations (Appendix 1). The main fluvial drainage out of the lake, the Lyre River, flows north into the Strait of Juan de Fuca.

The watershed surrounding Lake Crescent encompasses 130 km² with the majority of tributaries discharging into the lake intermittently as they dry up in late summer (Moran et al., 2013). There are only 5 or 6 perennial fluvial inputs to the lake and the largest, Barnes Creek discharges an average of 1.75 m³/s (Appendix 1; Fig. 4). The Barnes Creek delta has built outward from the southeastern shore of the southern basin and is the main site of fluvial input to the lake (Moran et al., 2013). Lake Crescent generally experiences a moderate, maritime climate without the precipitation and temperature extremes of higher elevations within the Olympic Mountains (Moran et al., 2013). Average precipitation ranges from ~140 to 190 cm annually with summer high temperatures ranging from ~18 to 24° C and winter temperatures fluctuating between ~1 and 9° C (Moran et al., 2013). Conifer trees are the main type of vegetation surrounding Lake Crescent with specific species varying with elevation; red alder trees are prominent along the shoreline of the lake where anthropogenic disturbance has occurred (Moran et al., 2013). The major transportation route of the north Olympic Peninsula, Highway 101 and over 100 private residences as well as three resort facilities and a National Park Service campground are located around the lake (Moran et al., 2013). Determining the geologic hazards associated with earthquakes on or near Lake Crescent is crucial to assessing the hazard risk for these developments.

3. METHODS

3.1 *Geophysical Data Collection*

The high resolution bathymetric survey of Lake Crescent was conducted using the R/V Snavely with a 100 kHz Reson 7111 multibeam system that returns both bathymetry and backscatter-intensity. Individual survey beams are 1.9° along-track and 1.5° across-track. Survey tracks were designed to give at least 25% overlap in coverage. Differentially Corrected Global Positioning System navigation data was passed through an inertial measurement unit to the system hardware and data collection software. A high-resolution CHIRP seismic reflection survey of Lake Crescent was conducted in May of 2013 using an Edgetech SB-512i system that operated at a 2-12 kHz sweep-frequency pulse with 20 ms duration. The instrument was suspended 1.25 m beneath the lake surface using a catamaran towed at a distance of 10 m behind a small boat. Tracklines were run at a

speed of ~2.5-3.0 knots. A WAAS-enabled GPS provided horizontal positioning with an accuracy of about 1-3 m. Two-way travel times were converted to depths by assuming a mean sound velocity of 1500 m s^{-1} (Jensen et al., 2011).

3.2 Sediment Core Collection

Fourteen sediment cores, ranging from 0.3 to 7.9 m in length, were collected from Lake Crescent in collaboration with personnel from LacCore, the National Lacustrine Core Facility at the University of Minnesota, using a Kullenberg Piston Corer in September 2015. The Kullenberg is a single-drive piston corer that is propelled into the sediment from the momentum of lead weights (up to 1000 pounds/450 kg) attached to the core head. Steel barrels lined with polycarbonate tubes collect the sediment. The weight atop the core barrel is triggered when the attached gravity corer, which is suspended to the side of the piston corer by a secondary line attached to the main cable, impacts the sediment surface and stops moving downward. The gravity corer is meant to collect the upper meter of sediment that can be disturbed by the longer corer. However, the gravity core system did not prove very effective in Lake Crescent, so that the upper centimeters to decimeters of the lake bed were not sampled at most locations. Five gravity cores ranging from 9 to 54 cm long were recovered from the smaller northern basin while two, 50 and 53 cm long were taken from the elongate southern basin. The core barrel is retrieved using a winch and hydraulic system. Recovering and deploying the long core barrels required the use of a tower erected atop two 19-foot, 950-pound skiff boats bolted underneath an aluminum platform. The retrieved piston cores were removed from the steel barrels, cut into 1.5 m sections, capped and labeled on shore (Fig. 5). They were then transported by truck to the LacCore lab in Minneapolis, Minnesota and placed in cold storage.

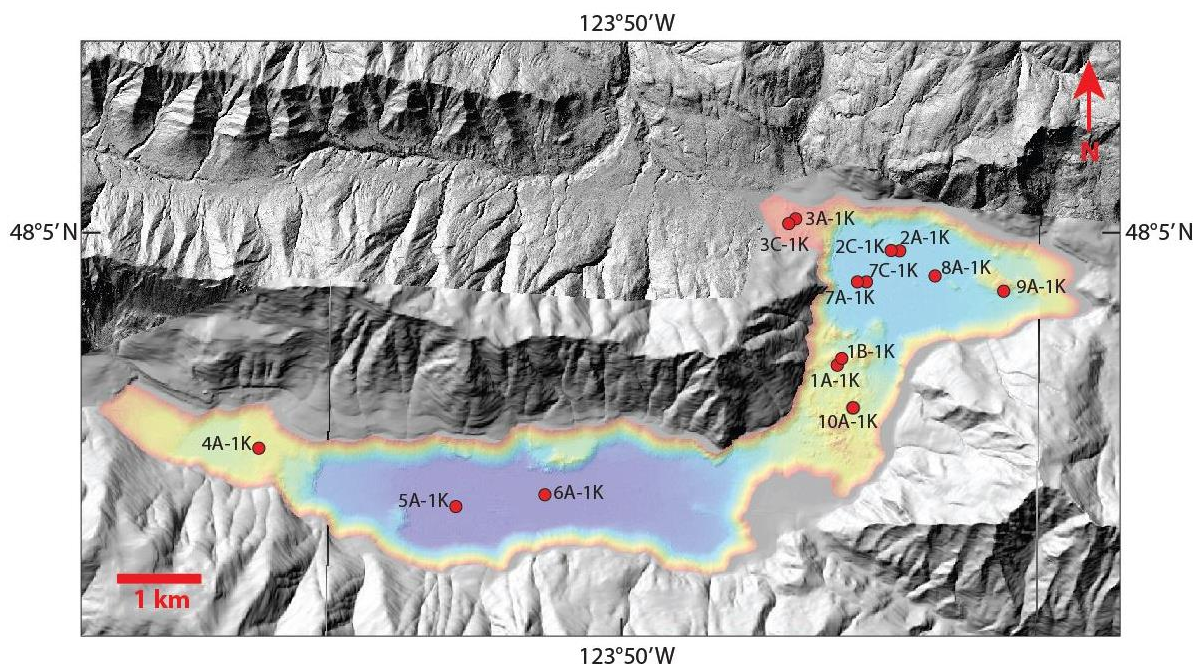


Figure 5. Kullenberg core collection sites on bathymetric map of Lake Crescent and topographic map of surrounding region (USGS, 2001; Puget Sound, 2015).

3.3 Sediment Core Processing

Initial core processing occurred at the LacCore laboratory facilities at the University of Minnesota approximately four weeks after core collection. Whole-core logging on the Geotek Multisensor Core Logger (MSCL) measured sediment density, acoustic wave velocity, electrical resistivity, and loop-sensor magnetic susceptibility at 1 cm resolution. Cores were then split into a working half and an archival half using vibrating medical cast saws, utility knives, and fishing line or filet knives. The surfaces of the split cores were smoothed with glass slides before being photographed and visually assessed. The working half was photographed at 10-pixels/mm resolution after calibration to known standards in order to achieve visibility of very fine details. The archival half was covered with non-reflective film and placed in the Geotek XYZ core scanner. This core scanner measures high-resolution point-sensor magnetic susceptibility as well as color data at 0.5 cm intervals. The working half was placed into a core cradle for visual analysis as well as sample collection. Samples for particles size and other analyses were taken at regular intervals (5-10 cm) as well as where interesting features were observed. Samples for radiocarbon (^{14}C) analysis were

collected where visible plant debris was present. After sampling, each half of the core was wrapped in plastic and placed into cold storage. Corelyzer 2.0 software was used to examine the core images at a DPI of 508 alongside magnetic susceptibility and density data for each core (Conze et al., 2010). PSICAT (Paleontological Stratigraphic Interval Construction and Analysis Tool) software was used to create and edit stratigraphic columns corresponding to each core image (Conze et al., 2010).

3.4 Particle Size Analysis

Approximately 100-200 mg of each sample collected for particle size analysis was placed into a 50 mL beaker with deionized water. An oblong magnet was placed into the beaker that was then set on a stir plate for ~2 minutes. Using a single use dropper, the contents were added to a Beckman Coulter 13-320 Laser Particle Size Analyzer equipped with a Universal Liquid Module to determine the sediment particle size in a range from 0.04 to 2000 μ m. Grain-size analyses were performed without chemical pre-treatment of the samples. Magnetic susceptibility was used as a proxy for grain size to obtain information about the particle size throughout the cores at 0.5 cm resolution (Fig. 6).

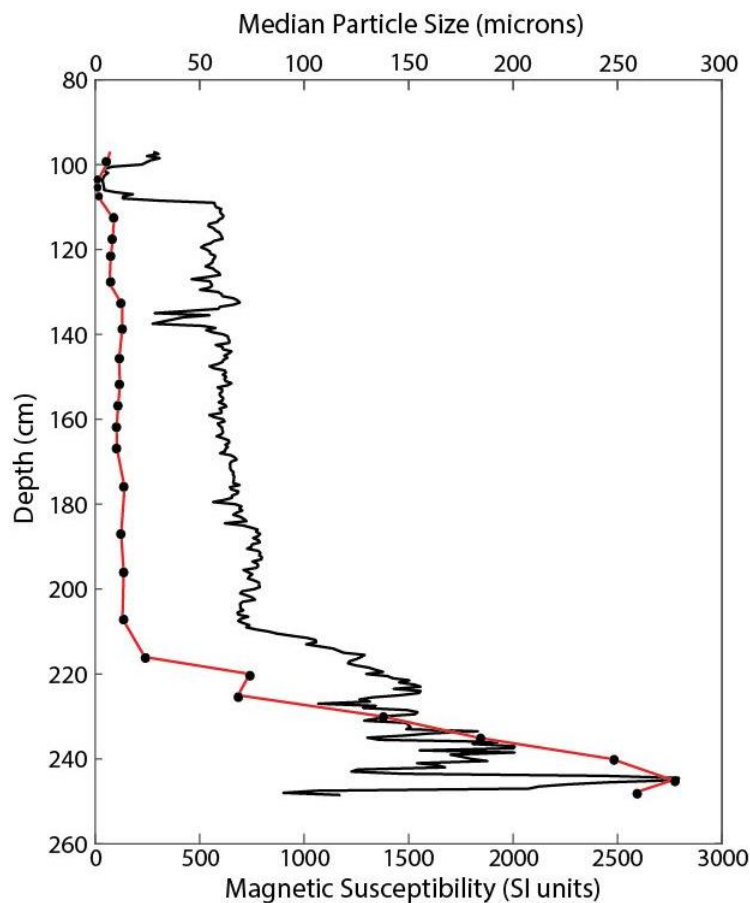


Figure 6. Median particle size (red) and magnetic susceptibility (black) for the thick event deposit present in core 2C-1K (depth 97-245 cm). The correlation coefficient between the two data sets is 0.84 indicating the two lines have a strong correlative relationship allowing the use of magnetic susceptibility as a proxy for grain size.

3.5 Radiocarbon Sample Processing

Samples of plant debris were pretreated by the Acid-Base-Acid (ABA) method before radiocarbon dating (Olsson, 1986). Nitrile gloves were worn at all times during the sample processing. Prior to contact with samples, all glassware used was fired in a programmed kiln held at a temperature of 550° C for about two hours. Metal-ware (sieves, tweezers) was washed in solvents (methanol and acetone) between each sample interaction. Thirty-seven samples were initially rinsed through a 63 micron stainless steel sieve with deionized water to remove adhered mineral particles. Material to be dated was carefully picked out with a tweezers, rinsed, and placed into a 50 mL glass beaker. Enough 1 N hydrochloric acid was added to each beaker to completely submerge sample

material, and the beakers were then placed in a 70° Celsius water bath for 30 minutes. After the time allotted, the hydrochloric acid was removed from the samples using a sterile syringe designated for use with each specific sample to avoid contamination. 1 N sodium hydroxide was then added to each beaker, completely submerging the sample, which was placed in a 70° Celsius water bath for 60 minutes. After an hour, the sodium hydroxide was removed using the designated syringes. The process of adding sodium hydroxide, placing the samples in a water bath, and removing the sodium hydroxide was repeated until the liquid in the beaker was clear. This process was repeated 5 to 35 times depending on the sample. After the final, clear sodium hydroxide was removed from the samples, 1 N hydrochloric acid was once again added to a level completely submerging samples. Beakers were then placed in a 70° C bath for 30 minutes. After half an hour the hydrochloric acid was removed and deionized water was added to each beaker. Samples containing the deionized water were placed in a 70° C water bath for 5 minutes before the deionized water was removed and replaced. This process was repeated 4 to 5 times until the water in the samples tested at a pH of 7. After the final deionized water was removed from the beakers, the neutralized samples were placed on a 40° C hot plate to dry, a process that took approximately 6 hours.

3.6 Age Models

The Bayesian-based age-modeling program, Bacon, was used on the software platform R with the IntCal13 ¹⁴C calibration curve (Blaauw & Christen, 2011). Bacon combines radiocarbon (and other) dates to reconstruct the Bayesian accumulation histories for sedimentary deposits. This program was used to model age versus depth for cores from which multiple radiocarbon dates were obtained. Bacon divides each core into sections of equal thickness, starting from the uppermost dated depth through the lowermost, and models accumulation rates for each of the sections (Blaauw & Christen, 2011). The range of section thicknesses used for the Lake Crescent cores was the maximum number of sections within the “safe range” (between 10 and 200 sections) prompted by Bacon. The ‘safe range’ falls in between too few sections where age-models will be generated with unrealistically abrupt bends and too many sections which may over-parameterize the model leading to an unresponsive age-model (Blaauw & Christen, 2011).

4. RESULTS

4.1 *Sedimentary Deposits*

Sedimentary deposits in the Lake Crescent cores include both material that accumulated relatively slowly, representing “background” or everyday sedimentation, and discrete layers that accumulated during episodic events. Background material in the cores is predominantly composed of faintly laminated to massive light brown to gray diatomaceous silt and does not appear to record seasonal variations in sediment discharge or productivity (i.e., they are not varved). These sediments most likely originate from settling in the water column of fine-grained stream and tributary-derived clastic particles mainly originating from Barnes Creek, by far the largest tributary to the lake. The highly diatomaceous silt is intercalated with millimeter to meter-scale sedimentary event deposits. An event layer is characterized by a significant change in the sediment accumulation within the lake such as a change in the type of sediment or processes by which material is deposited. Four main types of event layers were distinguished from the background lake sediment using the magnetic susceptibility and density profiles of the cores as well as visual analysis (Fig. 6).

The first type of sedimentary event layer deposit (EL1) distinguished from the background sediment range in thickness from 12 cm in core 4A-1K to an average of ~170 cm in cores obtained from the deep middle portions of both lake basins. In the basin centers, EL1 deposits are characterized by a sharp, erosive basal contact overlain by an average ~40 cm-thick-layer of coarse basaltic sand with faint laminations visible and common concentrations of terrestrial plant fragments near the base. The sandy unit grades upward into a homogenous, brownish-gray silt layer that is roughly 120 cm thick in the center of the basins and 7 to 18 cm thick on the edges of the lake. This layer is topped by a light gray clay cap of average ~8.5 cm thickness in the northern basin and ~2.6 cm thickness in the southern basin. High peaks in the magnetic susceptibility and density profiles correlate to the coarse basal sand units while the clay caps are characterized by low values (Fig. 6). Fairly consistent magnetic susceptibility values characterize the central, silt layer (Fig.6). Each clay cap is overlain by inter-stratified 1 to 5 mm thick chlorite, basaltic sand, and fine silty clay laminae except in cores retrieved from the shallower margins of the lake (4A-1K and 9A-1K).

The second type of event layer (EL2) present in the Lake Crescent stratigraphy is recognized as having a sharp, often erosive, basal contact. EL2 layers, in most instances, contain a roughly 1 to 2 cm thick (maximum 4 cm) basal layer consisting of massive to fining upward basaltic sand rarely with a few laminations. The basaltic sand is mixed with varying amounts of woody material, and then is topped by a unit of medium brown to dark gray silty sediment with fragments of wood interspersed. Magnetic susceptibility values peak where basaltic sand is present and decrease or remain stable through the layer above indicating that the overlying silt is normally graded or homogeneous. A few of the EL2 deposits have a <5 cm thick layer of light colored, fine clayey material overlying the central silt unit. EL2 layers range in thickness from 4 to 33 cm. They differ from EL1 deposits in that they are thinner and individual EL2 deposits can vary in sediment source material, grain size, and structure across the lake basins. EL2 deposits are thicker (average ~14 cm) in the deepest portion of the southern basin and thinner in the elevated and somewhat isolated western depression of the southern basin and in the northern basin (average ~4.5 cm).

The third identified event layer type (EL3) is distinguished by folded and contorted lacustrine sediment layers. The deformed material consists of thin, black basaltic sand layers, light brown and gray clay beds, and green clay to silt layers which are interbedded between the faintly laminated silty background sediments. The folded beds are separated from the under- and overlying horizontally-bedded sediments by distinct contacts. EL3 deposits range in thickness from 43 cm to 184 cm.

The final type of unique event layer (EL4) ranges in thickness from 23 to >160 cm and is characterized by poorly sorted clay to coarse pebble sized clasts intermixed with woody terrestrial plant debris. The magnetic susceptibility and density profiles associated with EL4 units are highly variable indicative of the range in particle size and type of material present throughout these deposits.

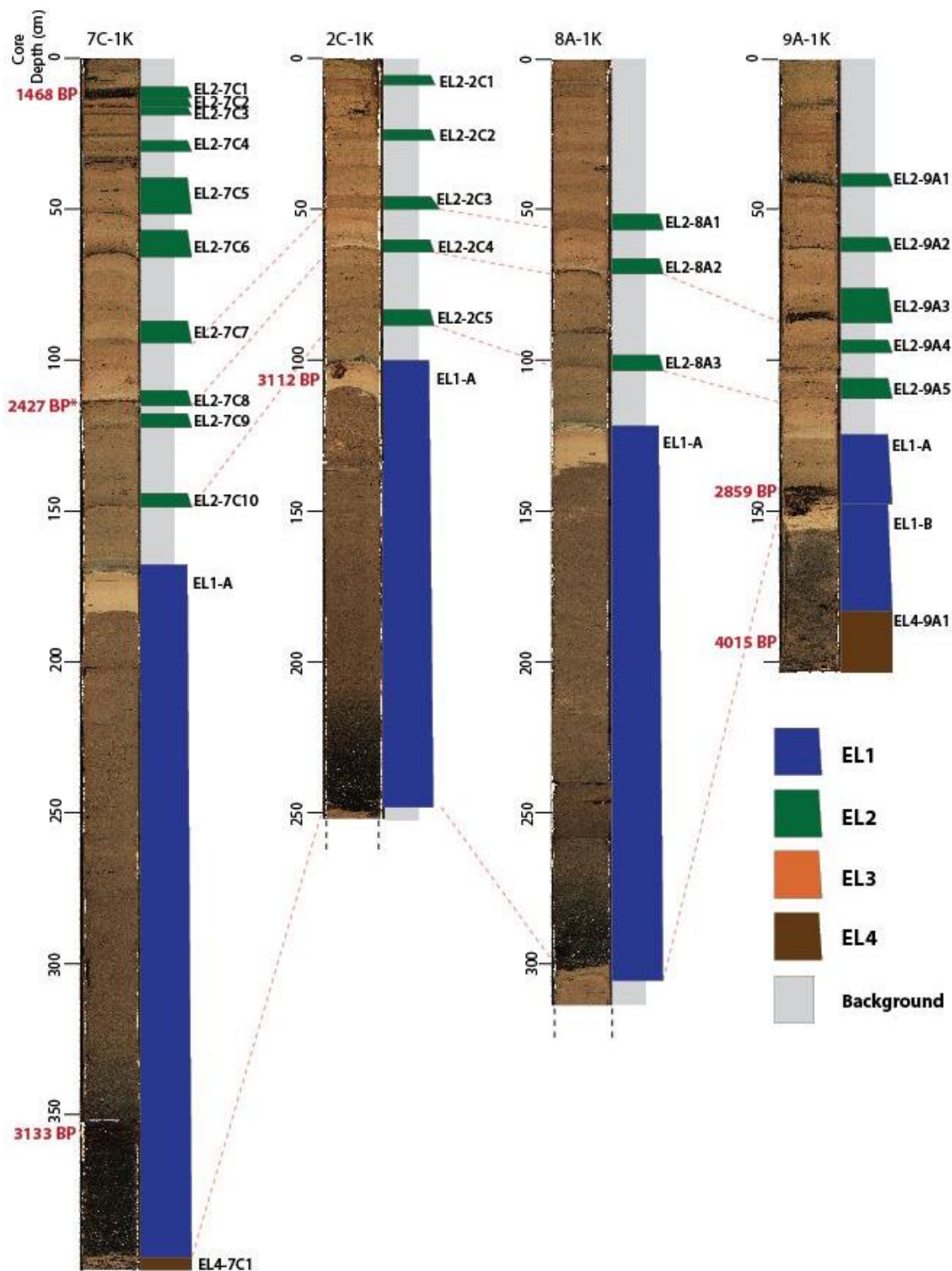


Figure 7a. Event layers correlated across the northern basin of Lake Crescent. Event layers are identified in the core images and their corresponding stratigraphic columns and correlated where possible. Dashed red lines correlate layers from the base of the deposit. Event layers are identified by their respective type, core ID, and order from top of each core; for example, EL2-4A1 is a type EL2 sedimentary deposit in core 4A-1K and is the uppermost EL2 unit recognized in the core. See Appendix 3 for a description of each event layer present in the sediment record.

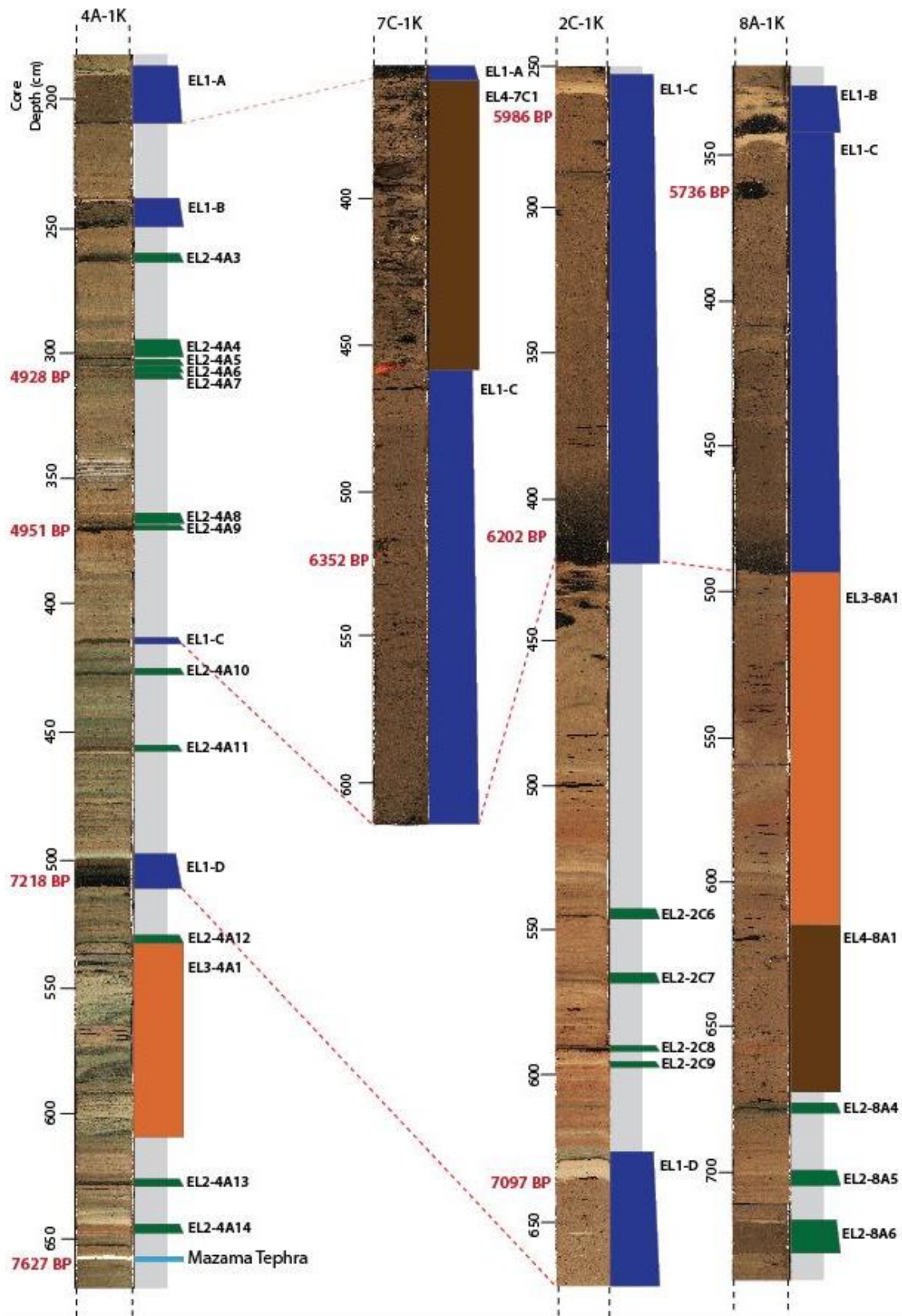


Figure 7b. Continued event layers correlated across the northern basin of Lake Crescent.

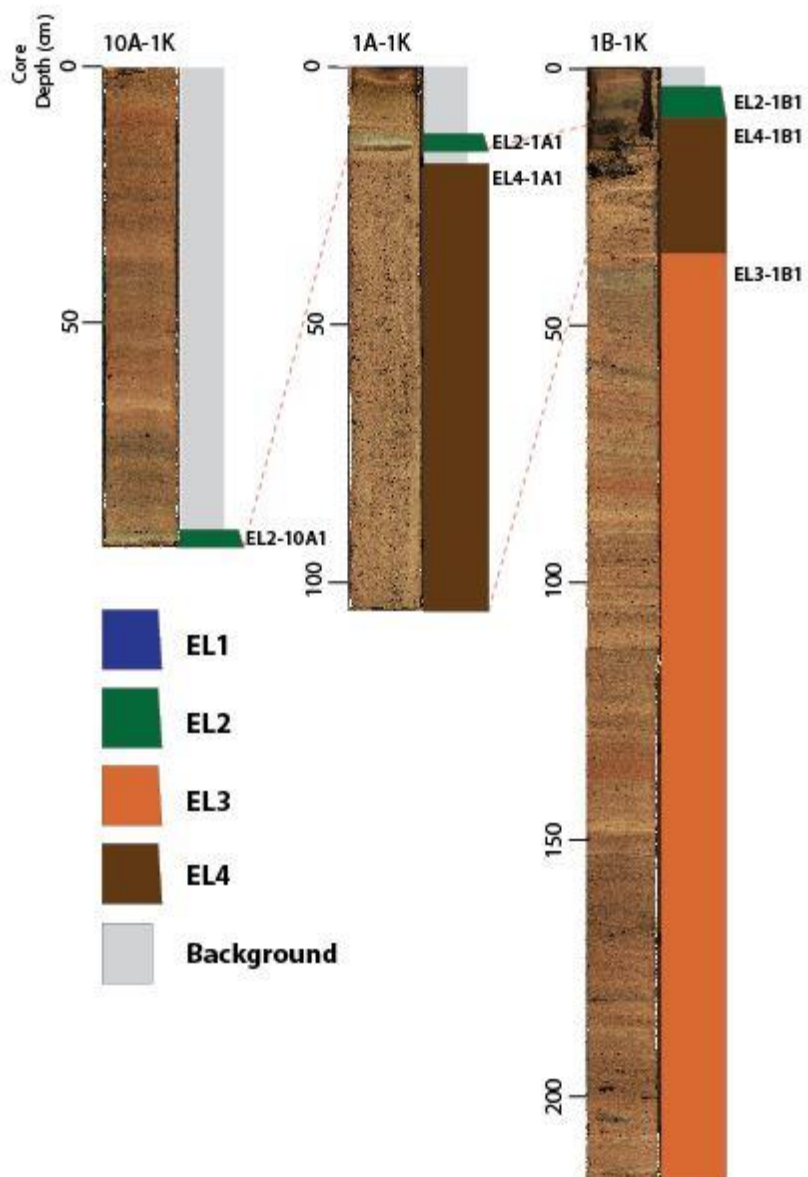


Figure 7c. Event layers correlated through the broad channel connecting the northern and southern basins in Lake Crescent.

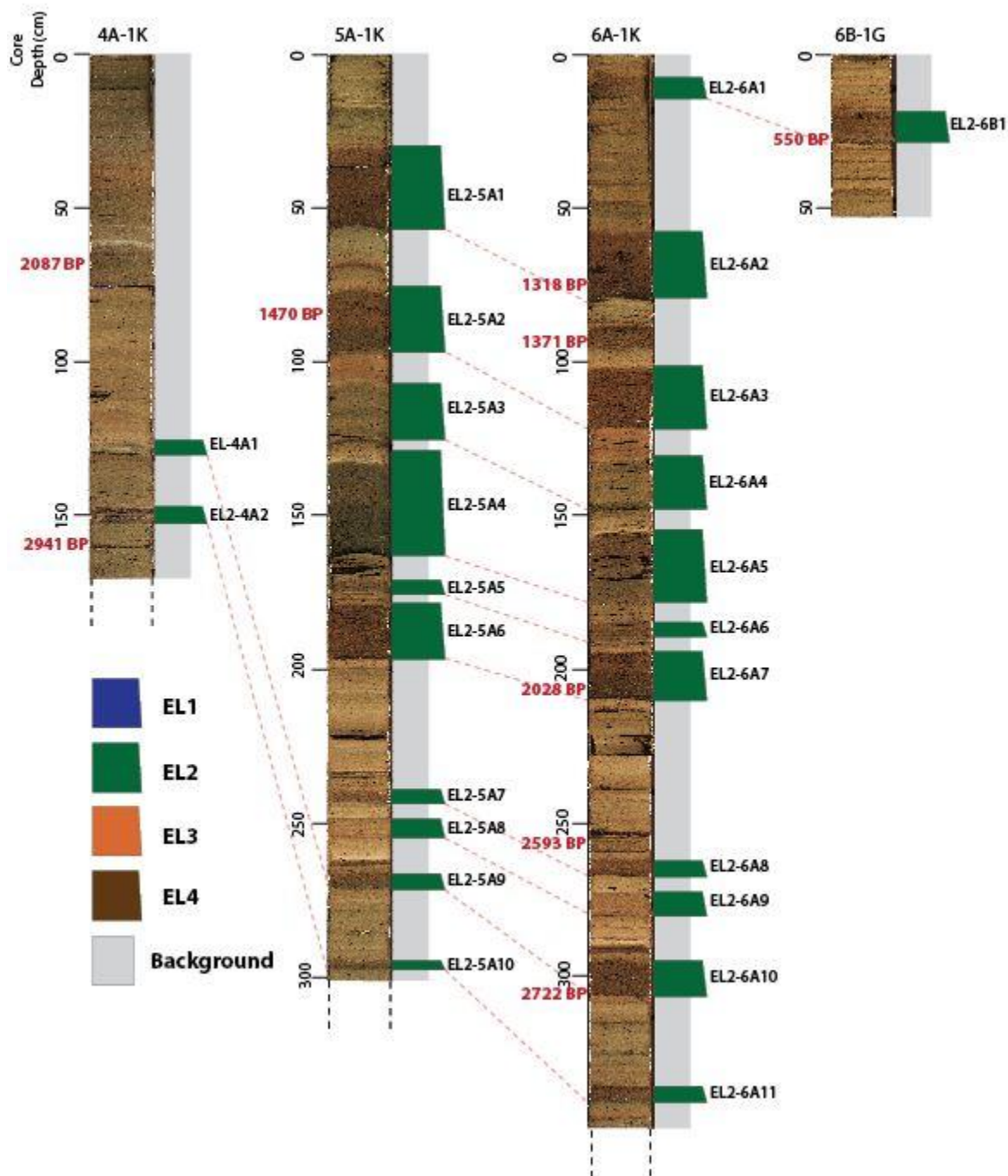


Figure 7d. Event layers correlated through the southern basin of Lake Crescent.

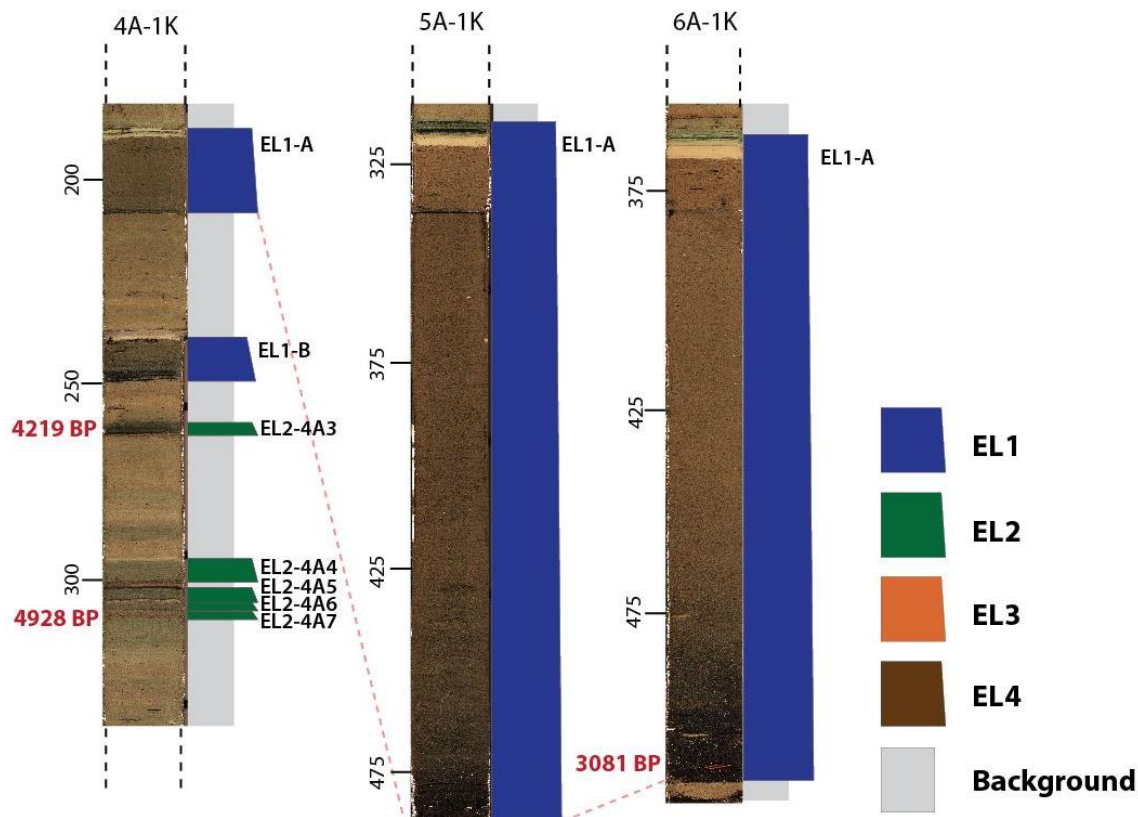


Figure 7e. Continued event layers correlated through the southern basin of Lake Crescent.

Four EL1 deposits are present in the lake sediment record and are designated EL1-A through -D. The stratigraphically uppermost EL1 deposit (EL1-A) ranges from 22 to 230 cm (average ~133 cm) thick and can be correlated throughout the lake from the southwest (core 4A-1K) to the northeast (core 9A-1K) (Figs. 7a, 7b, & 7e). The basal layer of EL1-A is located ~3 cm from the bottom of core 6A-1K while core 5A-1K did not penetrate deeply enough to collect the entire EL1-A deposit (Fig. 7e). The shorter length of these cores prohibits correlation of the additional three EL1 deposits to the deep center of the southern basin. However, the three additional EL1 units can be seen in the northern basin as well as in core 4A-1K. EL1-B is the least prominent of the EL1 layers and is only present in core 4A-1K, 8A-1K, and 9A-1K (Figs. 7a & 7b). EL1-C can be traced throughout the northern basin with an average thickness of ~174 cm and finally, the distinguishable top of a fourth layer, EL1-D, is seen in cores 2A-1K and 2C-1K (Fig. 7b).

Core 4A-1K, retrieved from the relatively shallow, westernmost depression in the southern basin, contains the greatest number of event layers and the longest sediment record. The only airfall

tephra layer present in the cores is located at 4.67 m event free depth in core 4A-1K (Fig. 7b). This core also contains the greatest number of EL2 deposits, 16, ranging in thickness from 2 to 9 cm thick, with an average thickness of ~4 cm (Figs. 7b, 7d, & 7e). Cores 5A-1K and 6A-1K, obtained from deep central locations within the southern basin contain 10 and 11 EL2 event layers, respectively, averaging ~14 cm thick, with a maximum of 33 cm thick (Fig. 7d). In the northern basin, between 3 and 10 EL2 layers of a 12 cm maximum thickness were sampled, and in the broad channel between the basins, only one 2 to 6 cm thick EL2 deposit was identified (Figs. 7a, 7b & 7c).

Each EL3 deposit, characterized by deformed lacustrine strata, is immediately overlain by another type of event deposit. In core 4A-1K, a 76-cm-thick EL3 layer lies directly underneath an EL2 deposit. Core 1B-1K, from the channel connecting the two basins of the lake, includes a 182-cm-thick EL3 deposit underneath a 27-cm -thick EL4 unit. In the shallow western portion of the northern basin, core 3C-1K, a 153-cm-thick EL3 layer is found directly underneath a 19-cm-thick EL4 unit. In the center of the northern basin, cores 7A-1K and 8A-1K contain EL3 deposits bracketed on top by EL1-A and EL1-C, respectively, and on the bottom by EL4 deposits. Core 7C-1K and 9A-1K contain EL3 layers overlying EL1-A and EL1-B, respectively.

Correlation between the Lake Crescent piston cores provides evidence for significant erosion during the events that deposited the EL1 layers. The absence of EL1-B from most of the cores suggests especially pronounced erosion during the emplacement of EL1-A. This scour is visible by the truncation of the underlying layers into the thicker chaotic to transparent homogenous layer representative of the EL1 deposits (Fig. 8; C. Joyner, NCSU M.S. thesis in progress). Prominent scour surfaces underneath the basal layers of EL1-A and EL1-C further indicate that erosion occurred which may have partially erased EL-B from the sediment record.

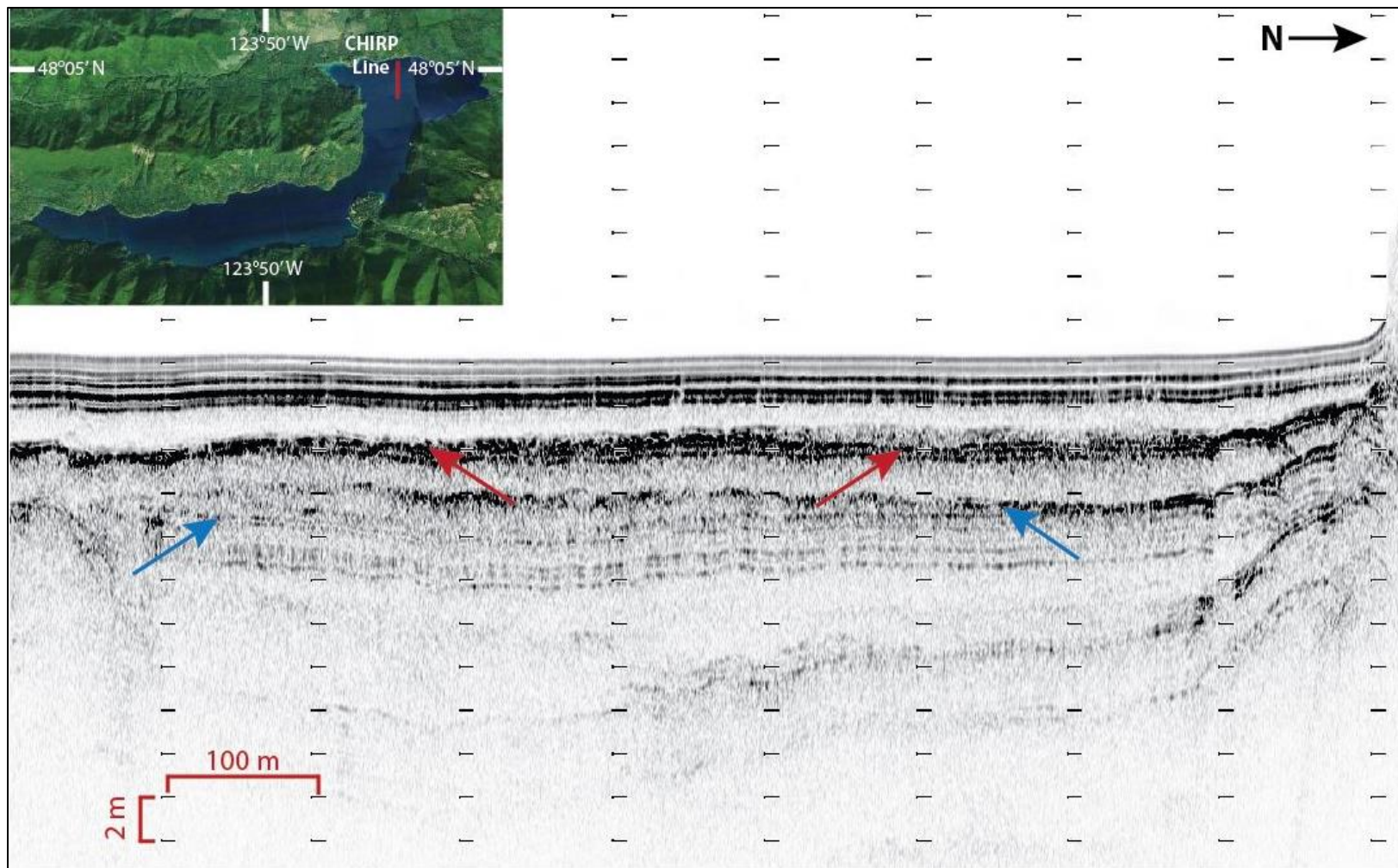


Figure 8. CHIRP seismic profile image obtained from the northern basin (see map inset). The two main scour surfaces are indicated by the red (EL1-A) and blue (EL1-C) arrows. The EL1 layers are recognized by their chaotic to transparent facies (Moernaut & De Batist, 2011). The identified scour surfaces are present where the EL1 facies truncate the high-amplitude to low amplitude, parallel and nearly horizontal reflections representative of background sedimentation with intercalated smaller event layers. Core 2C-1K was retrieved from near the center of the seismic profile.

4.2 Event-Free Depth

Event layers are deposited relatively instantaneously necessitating that their thickness be removed from the age model and accumulation rate calculations. The depth of each event deposit was subtracted from the total core thickness. The event-free depth (EFD) corresponds to the background sediment accumulation rate. Individual event layers reach up to ~2.0 m thick and comprise ~63% of the total sediment accumulation in the cored sediment record. The number of event layers in each core varies from a single event layer in core 10A-1K to 22 event layers in core 4A-1K.

Table 1. Event free length compared to core length for the 14 Lake Crescent Kullenberg cores.

Core ID	Core length (cm)	Event Free length (cm)	% Core Composed of Event Layers
1A-1K	104	11	89.4 %
1B-1K	218	3	98.6 %
2A-1K	526	173	67.1 %
2C-1K	679	254	62.6 %
3A-1K	32	14	56.3 %
3C-1K	262	86	67.2 %
4A-1K	780	611	21.7 %
5A-1K	487	166	65.9 %
6A-1K	522	218	58.2 %
7A-1K	670	89	86.7 %
7C-1K	654	115	82.4 %
8A-1K	791	284	64.1 %
9A-1K	205	104	49.3 %
10A-1K	93	91	2.2 %

4.3 Age Models and Accumulation Rates

Ages of individual event layers were determined using calibrated radiocarbon dates, accumulation rates and the Bacon-derived age models (Blaauw & Christen, 2011). ^{14}C dates were calibrated using Calib 7.0 with the IntCal13 curve (Reimer et al., 2013). Predominately woody debris collected from throughout the sediment cores produced 29 stratigraphically consistent radiocarbon ages (Table 2). A tephra layer located in the middle of a section of core bracketed by two radiocarbon dates of 7218 (7167-7267) cal BP and 8505 (8428-8587) cal BP is correlated to the eruption of Mount Mazama, which produced Crater Lake in modern day Oregon. The Mazama tephra is one of the few late Quaternary ash layers found on the Olympic Peninsula and anchors the ^{14}C dates at 6730 ± 40 ^{14}C years BP (7478-7620 cal years BP) (Hallet et al., 1997). Radiocarbon dates, including the age of the Mazama tephra, were used to determine Bacon age models for cores 4A-1K, 6A-1K and 7C-1K (Fig. 9).

Table 2. Lake Crescent radiocarbon dates. Dates marked with † indicate the date was stratigraphically inconsistent and therefore excluded from all age models.

Core ID	Sample Depth within Core Section (cm)	Dated Material	Event-free depth (cm)	Radiocarbon Age (1 sigma error)	Calibrated 95% age range (cal. yr BP)	Median cal. age of 95% confidence intervals
2A-1K-4	95-96	twig	129	5242 ± 31	5921-6177	5986 BP
2A-1K-5	23-24	wood and bark fragments	129	5378 ± 31	6021-6282	6202
2C-1K-1	100-105	twig with bark	89	2951 ± 29	3003-3208	3112
2C-1K-5	44.5-45.5	twig	253	6208 ± 33	7006-7242	7097
3C-1K-1	70-75	wood and bark fragments, leaves	22	5010 ± 63	5619-5902	5753
4A-1K-1	76.5-78	wood and bark fragments	72	2114 ± 29	1999-2285	2087
4A-1K-2	85.5-86.5	wood and bark fragments, needles	158	2835 ± 34	2859-3059	2941
4A-1K-3	2-3.5	wood and bark fragments	203	4121 ± 28	4530-4815	4653 [†]
4A-1K-3	26-26.5	wood and bark fragments	211	3827 ± 27	4100-4402	4219
4A-1K-3	71-72.5	wood and bark fragments	242	4370 ± 29	4530-4815	4928

Table 2. Continued

4A-1K-3	133-134	wood and bark fragments	290	4392 ± 33	4862-5047	4951
4A-1K-4	114-124	wood and bark fragments	391	6287 ± 30	7167-7267	7218
4A-1K-7	3-4	cone and bark fragments	547	7728 ± 40	8428-8587	8505
4B-1G-1	28-31	twig	16.5	539 ± 36	510-639	549
4B-1G-1	47-48	wood and bark fragments	34	1217 ± 26	1063-1240	1140
5A-1K-2	46-49	wood and bark fragments	46	1585 ± 29	1407-1541	1470
6A-1K-1	76-77	wood and bark fragments	40.5	1407 ± 38	1280-1375	1318
6A-1K-2	9-11	wood and bark fragments	49.5	1490 ± 22	1325-1409	1371
6A-1K-2	99-100	Wood and bark fragments	83	2208 ± 25	2151-2312	2233 [†]
6A-1K-2	116-117	wood and bark fragments	85	2060 ± 24	1950-2115	2028
6A-1K-3	33-34	wood and bark fragments	127	2519 ± 26	2493-2742	2593
6A-1K-3	81-82	wood and bark fragments	149.5	2551 ± 25	2506-2750	2722
6A-1K-4	140-141	wood fragments	187.5	2930 ± 36	2963-3179	3081
6B-1G-1	28-30	wood and bark fragments	14.5	949 ± 27	796-925	854
6B-1G-1	37-38	wood, bark fragments	14.5	543 ± 32	514-636	550
7A-1K-1	85	cone fragments	99	2408 ± 28	2352-2681	2427
7C-1K-1	11-12	wood and bark fragments	9	1559 ± 26	1393-1526	1468
7C-1K-4	2-6	roots, twigs, bark fragments	153.5	2968 ± 27	3037-3226	3133
7C-1K-5	53-58	twig	153.5	5560 ± 40	6289-6411	6352
8A-1K-4	92-94	wood and bark fragments	107	5007 ± 28	5656-5889	5736
8A-1K-7	21-22	wood and bark fragments	4106 ± 25	4106 ± 25	4526-4810	4619 [†]
9A-1K-2	41-50	twigs with bark	120.5	2766 ± 28	2785-2943	2859
9A-1K-2	98-100	woody debris, bark fragments	120.5	3673 ± 27	3921-4088	4015

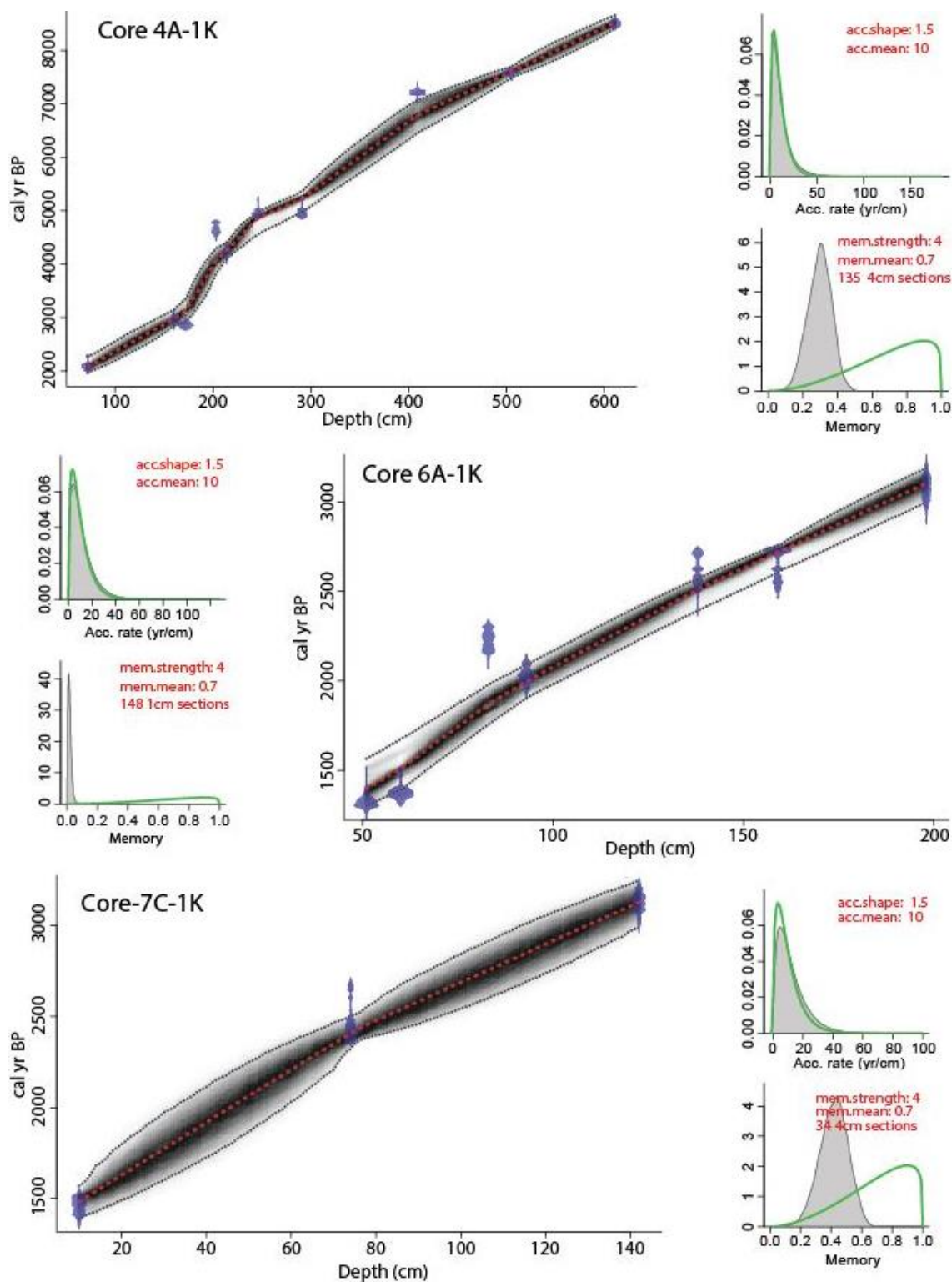


Figure 9. Age models interpolated from the Bayesian age modeling program Bacon for cores 4A-1K, 6A-1K, and 7C-1K. The calibrated ^{14}C dates are shown in transparent blue while the darker portions of the age-depth model indicate more likely calendar ages. 95% confidence intervals are demarcated by the dotted gray lines while the red curve indicates the 'best' model based on the weighted mean age for each depth (Blaauw & Christen, 2011).

Due to the erosive nature of piston coring, it is inferred that several centimeters to decimeters of sediment at the top of each piston core is missing. Thus, accumulation rates cannot be calculated from the top of the core. Accumulation rates for individual cores with radiocarbon dates were calculated for intervals in between the radiocarbon ages using their respective event free depths (Appendix 2). Representing the deep middle of the southern basin, cores 5A-1K and 6A-1K produced event-free sediment accumulation rates of 0.66 (0.60-0.75) mm/yr and 0.84 (0.77-0.94) mm/yr, respectively; range in parentheses represents accumulation rates calculated using two sigma calibrated age values. Core 4A-1K, from the shallower western portion of the southern basin, has an accumulation rate of 0.79 (0.76-0.82) mm/yr. The only core taken from the northern basin with enough widely dispersed radiocarbon ages, 7C-1K, produced a rate of 0.79 (0.72-0.87) mm/yr. These accumulation rates are fairly consistent with an event-included average rate of 0.79 mm/yr calculated by Moran et al. (2013) from sediment cores recovered using a 3.0 m long, 13 x 13 cm square Kasten coring device. This average was determined using radiocarbon dates from two <3 m sediment cores which produced accumulation rates of 0.93 and 0.84 mm/yr for the southern basin and 0.60 mm/yr for the northern basin, respectively (Moran et al., 2013).

5. EVENT LAYER HISTORY AND CORE STRATIGRAPHY

5.1 Megaturbidites

As previously noted, the four EL1 deposits present in the lake sediment record are characterized by three superposed units. First, an erosive surface is overlain by a fining-upward, coarse basal layer, which is topped by a thick homogenous silty unit, and finally capped by a layer of clay (Fig. 10). Siegenthaler et al. (1987) described similar beds in lacustrine deposits in the French Alps, which they termed 'homogenites', and attributed to past earthquakes. In later paleoseismic studies, similar beds have been termed megaturbidite deposits and were correlated to past earthquake events (e.g. Chapron et al., 1999, Fanetti et al., 2008, Hilbe & Anselmetti, 2014, Moernaut et al., 2014, among others).

The four megaturbidites present in the Lake Crescent record were identified by their exceptional thickness, much thicker than any other event layer in the sediment record, and by their

magnetic susceptibility profiles that reflect distinctive grain size shifts similar to those described by Chapron et al., 1999, Schnellmann et al., 2005, and Schnellmann et al., 2006. These thick, predominately homogenous layers can be correlated throughout the lake using seismic data as further indication of their broad extent and large volume (C. Joyner, NCSU M.S. thesis in progress). The average thickness of the megaturbidite layers is ~1.3 m with a maximum thickness of 2.3 m for the uppermost megaturbidite present in core 7C-1K. The deposits are thickest (>1.5 m) in the deep center of both basins and thinner (13 to 28 cm) in the shallower margins of the lake represented by cores 4A-1K and 9A-1K.

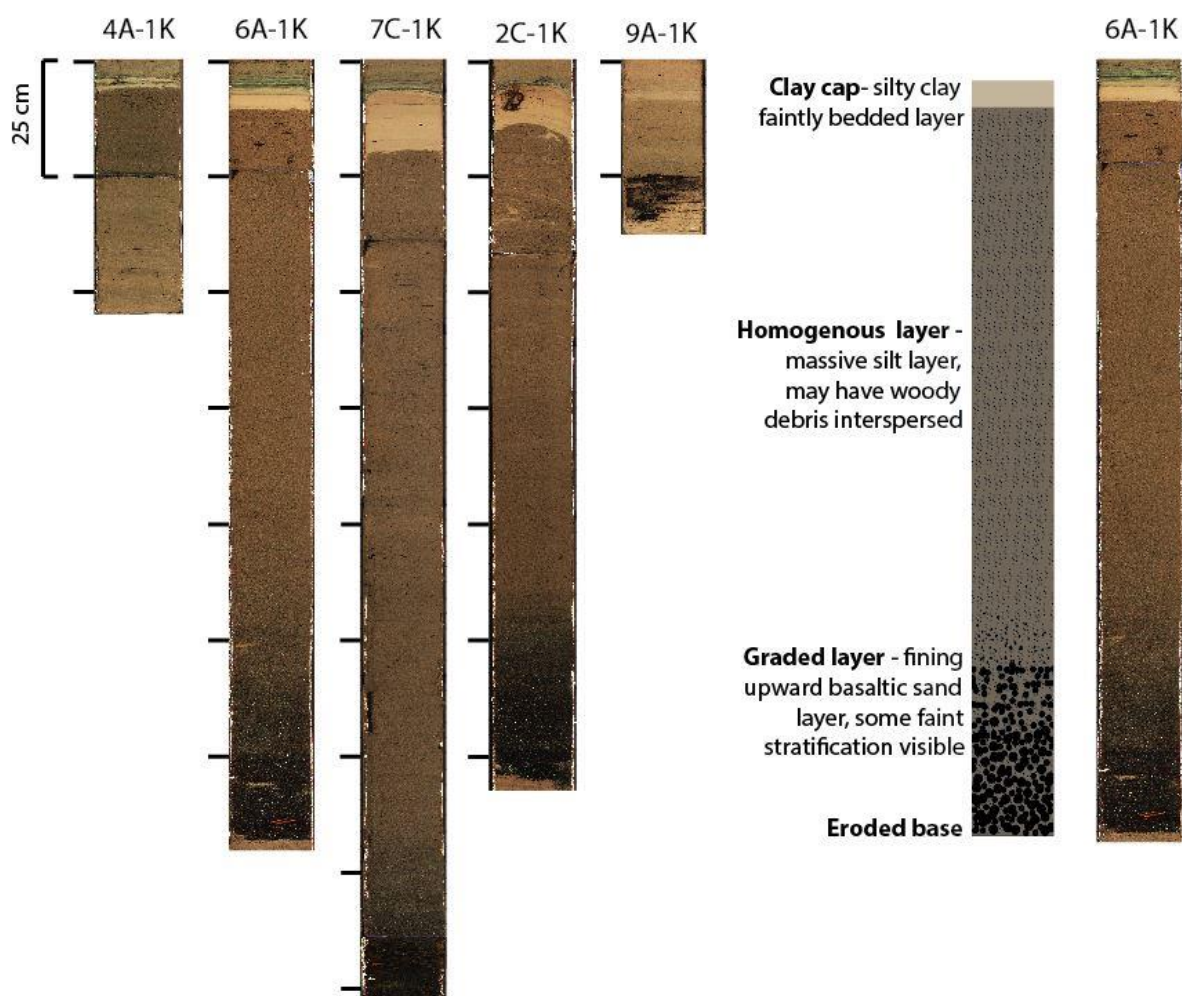


Figure 10. Five core images depicting the uppermost megaturbidite (EL1-A) deposit with a description of the typical megaturbidite facies observed in Lake Crescent. Core images are arranged from west to east across the lake. The thin layers of basaltic sand and chlorite-rich clay interlayered at the top of the clay caps may represent mobilization of material from the exposed landslide scarp during high precipitation events in the weeks to years following the initial, parent earthquake.

Terrestrial plant material was used to determine ages for the four megaturbidite deposits present in the record (Table 2). The macroscopic organic material (mainly wood and bark fragments) used for radiocarbon analyses was most likely remobilized into the lake during the erosive formation of the megaturbidites and may be decades, or more, older than the emplacing events. This results in an 'inbuilt age' defined as the difference between the time the wood material formed and the age of the event that transported the debris (Gavin, 2001). While an effort was made to date twigs and wood layers near the surface of the branch or log it is possible that some fragments were from older growth located within the wood material. This may also contribute to an older event date than indicated by the radiocarbon age. Therefore, the youngest age given for an event layer is assumed to be the maximum age of the event.

The median age of 2859 (2785-2943) cal yr BP, obtained from organic material taken from the basal layer of the megaturbidite in core 9A-1K is used for the widely correlated uppermost deposit (EL1-A). The maximum median age for this layer was 3133 (3037-3226) cal yr BP from core 7C-1K. The base of core 9A-1K gave a calibrated radiocarbon age of 4015 (3921-4088) cal yr BP for EL1-B. Woody debris from the top of the homogenous silty layer in the third megaturbidite deposit (EL1-C) yielded a calibrated age of 5736 (5656-5889) cal yr BP while woody material from the same layer in core 3C-1K gave an age of 5753 (5619-5902) cal yr BP. Organic debris from the clay cap of the oldest megaturbidite present in the retrieved sediment record (EL1-D) produced an age of 7097 (7006-7242) cal yr BP. Near the margins of the lake as well as shallow portions of the lake floor (cores 4A-1K and 9A-1K), the megaturbidite deposits tend to be thinner and the sandy basal unit pinches out. The scour shown in the CHIRP profile as well as the eroded base of the megaturbidite layers suggests the possibility that there may have been additional event layers that were removed from the Lake Crescent stratigraphic record entirely (Fig. 8).

Lacustrine megaturbidite event layers have been identified in many earthquake prone areas including Lake Lucerne, Switzerland (Hilbe & Anselmetti, 2014), Lake Le Bourget, France (Chapron et al., 1999), Lake Como, Italy (Fanetti et al., 2008), lakes in south central Chile (Moernaut et al., 2014 & Van Daele et al., 2015), and Lake Biwa, Japan (Inouchi et al., 1996). Megaturbidite deposits were identified in at least four Chilean lakes following the 1960 magnitude 9.5 Valdivia earthquake

(Van Daele et al., 2015). These megaturbidites were >1.0 m thick and defined by a coarse-grained base with a thick layer of homogenous mud on top, overlain by a fine-grained cap. In each of these lakes, the earthquake triggered one or more subaerial landslides and/or sub-lacustrine mass transport deposits that remobilized material into or within the lake creating large waves (lake tsunamis) and subsequent oscillations of the water column (lake seiches) (Van Daele et al., 2015). Bystanders confirmed the occurrence of the tsunamis and following seiches during and after the ground-shaking event. Large waves were reported on several additional lakes, but in these locations the initial wave was not followed by oscillatory movements and therefore a lake seiche did not occur. Lakes that did not experience the prolonged water movement from the seiche did not preserve a megaturbidite deposit. Hence, it was determined that a seiche is necessary to form a megaturbidite layer (Chapron et al., 1999; Schnellmann et al., 2005; Bertrand et al., 2008; Mulder et al., 2009; Van Daele et al., 2015). The thick, homogeneous silty layer that comprises the bulk of each megaturbidite is interpreted to require prolonged movement of the water column, which maintains reworked lake sediments in suspension (Beck, 2009). Reports of the M_w ~6.2 earthquake event that shook central Switzerland in 1601 indicate these oscillations of the water column lasted several hours after the initial event which triggered two large slump deposits within Lake Lucerne (Cysat, 1601; Siegenthaler et al., 1987). This earthquake event was determined to have generated megaturbidites as thick as 2 m in two separate subbasins (Schnellman et al., 2002). A similar series of events is inferred to have generated the megaturbidite deposits in Lake Crescent.

5.2 Turbidites

EL2 layers are interpreted to be turbidite deposits because of their distinct, most likely erosive, base and homogenous to fining upward grain size structure. However, the variable grain size structure and multiple mechanisms of formation associated with these deposits make it difficult to determine a definite type of event origin. Turbidites may have formed in Lake Crescent through several mechanisms, including earthquake triggered remobilization of sediment on the lake margins and deltas and episodic flood events. It is possible that some of the identified EL2 deposits represent input from streams during periods of heavy rainfall or rapid snowmelt from the higher elevation

portions of the catchment; however, the lack of large fluvial input sources to the lake argues against this as the sole cause. During floods, inflowing tributaries may carry a high enough sediment load to form a hyperpycnal flow into the lake. Hyperpycnites are distinguished by a fining upward grain size profile representative of the waning of the discharge or sometimes a coarsening upward basal unit from increasing underflow velocity during the initiation of a flood (Gilli et al., 2013). These types of deposits are composed of predominately terrigenous material transported from the stream or tributary mouths and tend to be coarser grained than the background sediments with a wide grain size distribution. However, episodic floods of the small tributaries and streams spilling into Lake Crescent seem unlikely to have produced the centimeter to decimeter-scale layers observed in the sediment record given the small size of the stream catchments surrounding the lake (Appendix 1).

In addition, within the southern basin, many of the EL2 deposits do not appear to decrease in thickness across the lake floor over the ~1 km between core 6A-1K and 5A-1K which would be expected of a flood induced turbidite triggered by a point source at, for example, Barnes Creek. It is interesting to note that the two thickest EL2 deposits in the southern basin are in core 5A-1K, not core 6A-1K which is closer to the most likely point source of terrestrial sediment input. Cores collected from the southern basin contain a greater number of thin (<2 cm) fine sandy layers that may record the episodic influx of sediment from Barnes Creek or the other drainages that are more prevalent in the larger, southern basin compared to the northern basin (Appendix 1).

The substantial thickness of the EL2 layers lends credence to a non-flood origin. The significance of each EL2 layer thickness can be determined by comparing the background annual amount of sediment discharged into Lake Crescent to the amount of material transported fairly instantaneously to create the EL2 deposits. The approximate watershed area that drains overland into Lake Crescent is 70 km², with the Barnes Creek sub-catchment accounting for ~60% of the total upland area (Appendix 1). Using the estimated suspended sediment yield for the nearby Hoh River, ~110 ton/km²/yr (Milliman & Farnsworth, 2011), the total approximate amount of sediment discharge from the creeks flowing into Lake Crescent is estimated at 7,700 tons/yr. This is a maximum estimate for Lake Crescent as the Hoh River drains recently deglaciated areas, the basin slopes are steeper and the surrounding rocks are not as competent as those around Lake Crescent. Therefore, the

annual suspended sediment yield into Lake Crescent is most likely less than the maximum estimate of ~7,700 tons/yr. Using only the drainage area for streams flowing directly into each basin the annual sediment discharge was calculated for both the north (385 ton/yr) and south basins (7,370 ton/yr; Appendix 4). This may not be representative of the somewhat isolated western portion of the southern basin as some sediment is likely trapped on either side by the shallower landslide deposits separating the area from the main basin. Therefore, one half of the total sediment discharge from creeks flowing into the southern basin was used in conjunction with the discharge amount from the two tributaries flowing directly into the western depression for calculations involving core 4A-1K. However, it seems more likely that sediment was transported out of the isolated depression into the deeper basin; therefore, the sediment yield from the two tributaries flowing into the shallower depression was included in the average annual sediment yield calculations for the entire southern basin (Appendix 4).

In the southern basin, ten EL2 units can be correlated between cores 5A-1K and 6A-1K, which are ~1 km apart in the center of the deepest part of the basin (Fig. 5). These correlated event layers range from 4 to 33 cm with an average thickness of ~14 cm. Using the area of the flat bottom of the southern basin (where EL2 layer thickness is inferred to be consistent) and assuming a porosity of 40%, it is estimated that between 5.63×10^5 and 4.65×10^6 (average 1.97×10^6) tons of sediment were deposited during a single EL2 forming event (Appendix 4). This converts to between 77 and 631 (average 268) years of average sediment yield represented by each EL2 deposit in the southern basin (Appendix 4). For the smaller northern basin, the average EL2 layer thickness is ~4.5 cm, with a range of 3 to 12 cm. Using the aforementioned 40% porosity and area of the flat bottom of the northern basin, the amount of sediment deposited instantaneously during a single EL2 event ranges from 2.30×10^5 to 9.19×10^5 (average 4.47×10^5) tons which represents 596 to 2386 (average 895) years of sediment accumulation in the northern basin (Appendix 4). It cannot be discounted that at least some of the thinner layers may represent large hydrologic flood events (e.g. 100 year RI floods), but the thick layers that represent upwards of 100 years of sediment yield deposited fairly instantaneously most likely have a different origin, such as earthquake triggered remobilization of sediment perched on deltas and steep slopes around and within the lake.

Previous research of flood layers within Lake Quinault, located ~50 km south of Lake Crescent on the Olympic Peninsula, found flood events left mm to cm thick hyperpycnal flow deposits (Smith, 2016). These flood layers are thinner than the turbidites in Lake Crescent even though the average annual rainfall in the Quinault region is about five times greater than at Lake Crescent and the major tributary flowing into Lake Quinault, the Quinault River, drains a catchment of ~ 600 km² compared to the ~70 km² area draining into Lake Crescent (Moran et al., 2013; Smith, 2016). The comparatively smaller size of the flood event layers as well as the location of the two lakes in regards to average rainfall and the difference in their catchment areas provides further indication that the turbidites in Lake Crescent are not from large flood events.

Individual EL2 layers were correlated visually, taking into account their respective ages, and grouped into 19 Lake Crescent Turbidite layers (LCT) (Table 3 & Figs. 7a-e, 12, & 13). These 19 LCT layers are tentatively assigned a seismic origin due, in part, to their substantial thickness that is representative of greater than 100 years of estimated annual suspended sediment yield. It also appears that several of the EL2 deposits may contain sediment from more than one source, which is indicative of a mechanism that triggered remobilization of material in multiple locations, such as an earthquake. However, further analysis of the mineralogy of the EL2 layers is necessary to determine the exact origin of their sedimentary components. Additionally, several subaqueous mass wasting deposits are visible on the lake margins (Fig. 4). While these failures may have occurred in the absence of earthquakes, earthquakes have been shown to trigger failure of underwater slopes and remobilization of surficial sediments; therefore, seismic events must be considered a likely trigger for the formation of EL2 layers in this tectonically active area (e.g., Moernaut et al., 2015; Van Daele et al., 2015)

Table 3. Description of the nineteen LCT (Lake Crescent Turbidite) event layers. Identified EL2 layers were visually correlated throughout the sediment cores and attributed to the same lake-wide turbidite event (LCT) if they shared a similar age and were visually comparable. Each of the LCT event layers include at least one EL2 deposit that represents over 100 years of annual sediment yield. Ages shown in red lettering were obtained through radiocarbon dating of organic material while ages marked by † indicate an age interpolated using Bacon. Ages determined from accumulation rates are bracketed by parentheses. The youngest age determined from an EL2 layer was used for the age of the LCT event layer.

LCT	Event Layer (correlated EL2 deposits represent one lake wide LCT unit)	Event Layer Thickness (cm)	Event Layer Age*	Average Tons of Sediment	Years of Sediment Yield Represented
LCT1	EL2-6A1; EL2-6B1	7 (S. Basin)	854 (796-925)	9.9x10 ⁵ (S. Basin)	134 (S. Basin)
LCT2	EL2-5A1; EL2-6A2	24-27 (S. Basin)	1318 (1280-1375)	3.6x10 ⁶ (S. Basin)	459-516 (S. Basin)
LCT3	EL2-5A2; EL2-6A3; EL2-7A1; EL2-7C1; EL2-2A1	2-6 (N. Basin) to 21 (S. Basin)	1468 (1393-1526)	2.6x10 ⁵ (N. Basin) 3.0x10 ⁶ (S. Basin) 3.6 x10 ⁶ (both basins)	596-795 (N. Basin) to 402 (S. Basin)
LCT4	EL2-5A3; EL2-6A4; EL2-7A4; EL2-7C4;	3-4 (N. Basin) to 17-21 (S. Basin)	1601† (1469-1765)	2.7x10 ⁵ (N. Basin) 2.7x10 ⁶ (S. Basin) 3.0 x10 ⁶ (both basins)	596-795 (N. Basin) to 325-402 (S. Basin)
LCT5	EL2-5A4; EL2-6A5; EL2-7A5; EL2-7C5;	6-12 (N. Basin) to 25-33 (S. Basin)	(1682)	6.9x10 ⁵ (N. Basin) 4.1x10 ⁶ (S. Basin) 4.8 x10 ⁶ (both basins)	596-2386 (N. Basin) to 478-631 (S. Basin)
LCT6	EL2-5A6; EL2-6A7; EL2-9A1;	2-4 (N. Basin) to 15-19 (S. Basin)	2028 (1950-2115)	2.3x10 ⁵ (N. Basin) 2.4x10 ⁶ (S. Basin) 2.6 x10 ⁶ (both basins)	795 (N. Basin) to 287-363 (S. Basin)
LCT7	EL2-7A7; EL2-7C7; EL2-2A2; EL2-2C3; EL2-8A1	3-6 (N. Basin)	(2137)	3.8x10 ⁵ (N. Basin)	596-1193 (N. Basin)
LCT8	EL2-7A8; EL2-7C8; EL2-2A3; EL2-2C4; EL2-8A2; EL2-9A3	3-6 (N. Basin)	2427 (2352-2681)	3.3x10 ⁵ (N. Basin)	398-994 (N. Basin)
LCT9	EL2-5A8; EL2-6A9; EL2-7A9; EL2-7C9 EL2-9A4	2-5 (N. Basin) to 8-9 (S. Basin)	2528† (2436-2660)	2.3x10 ⁵ (N. Basin) 1.2x10 ⁶ (S. Basin) 1.4 x10 ⁶ (both basins)	398-994 (N. Basin) to 153-172 (S. Basin)
LCT10	EL2-4A1; EL2-5A9; EL2-6A10; EL2-7A10; EL2-7C10; EL2-2C5; EL2-8A3; EL2-9A5	2-8 (N. Basin) to 5-11 (S. Basin)	2722 (2506-2750)	2.9x10 ⁵ (N. Basin) 1.1x10 ⁶ (S. Basin) 1.4 x10 ⁶ (both basins)	398-2386 (N. Basin) to 115-210-(S. Basin)
LCT11	EL2-4A2; EL2-5A10; EL2-6A11	4-6 (S. Basin)	2904† (2752-3080)	7.7x10 ⁵ (S. Basin)	77-184 (S. Basin)

Table 3. Continued.

LCT12	EL2-4A4	7 (S. Basin)	4839 [†] (4548-4949)	1.1x10 ⁶ (S. Basin)	215 (S. Basin)
LCT13	EL2-4A8	4 (S. Basin)	5220 [†] (4971-5362)	6.1x10 ⁵ (S. Basin)	123 (S. Basin)
LCT14	EL2-4A10; EL2-8A5	5 (N. Basin) to 3 (S. Basin)	5888 [†] (5596-6181)	3.8x10 ⁵ (N. Basin) 4.6x10 ⁵ (S. Basin) 8.4 x10 ⁵ (both basins)	994 (N. Basin) to 92 (S. Basin)
LCT15	EL2-8A6	12 (N. Basin)	(6204)	9.2x10 ⁵ (N. Basin)	2386 (N. Basin)
LCT16	EL2-8A7	7 (N. Basin)	(6901)	5.4x10 ⁵ (N. Basin)	1392 (N. Basin)
LCT17	EL2-4A14	6 (S. Basin)	7544 [†] (7411-7656)	9.1x10 ⁵ (S. Basin)	184 (S. Basin)
LCT18	EL2-4A15	6 (S. Basin)	7800 [†] (7655-7958)	9.1x10 ⁵ (S. Basin)	184 (S. Basin)
LCT19	EL2-4A16	9 (S. Basin)	8247 [†] (8086-8406)	1.4x10 ⁶ (S. Basin)	276 (S. Basin)

Due to the nature of piston coring, which may not preserve the upper decimeters of the lake sediments, it is probable that some of the uppermost EL2 layers are missing from the recovered sedimentary lake record. Similar radiocarbon ages of 1468 cal yr BP and 1470 cal yr BP were measured from near the tops of core 7C-1K, in the northern basin, and core 5A-1K, in the southern basin, respectively. However, the wood and bark fragments from the southern basin were collected from 11 cm EFD while the woody debris from the northern basin was obtained from 50.5 cm EFD. Therefore, assuming an equal “inbuilt-age” for the material, it is estimated that more of the sediment record was lost (not recovered) from the top of core 7C-1K than from core 5A-1K, and that younger event layers were not recovered in the northern core. Based on a calculated average accumulation rate of 0.79 mm/yr for the southern basin, it is estimated 50 to 60 cm of material is absent from the top of core 5A (Appendix 5). Similar calculations for the cores retrieved from the northern basin suggest that between ~100 to 130 cm (core 2C-1K may be missing up to ~200 cm) of the uppermost sediment record was not recovered (Appendix 5). This prohibits knowing the age of the most recent event layers as well as the total number of EL2 deposits in the sediment record without additional core retrieval.

5.3 Landslide and Slump Deposits

The folded EL3 deposits can be ascribed to subaqueous slump events. These event deposits range in thickness from 16 cm in core 7C-1K to 182 cm in core 1B-1K and are composed of folded and contorted, interbedded thin basaltic sand and silty clay background lake sediments (Fig. 11). Every recorded slump deposit (EL3) is found directly underneath a post-dating additional event layer without any background sedimentation present between the layers. In cores 3C-1K and 8A-1K slump deposits are found directly underlying the EL1-C event layer. This indicates that after the slump deposit formed little to no time passed before an additional event occurred depositing a sedimentary event layer, such as a megaturbidite (e.g. EL1-C). Multiple slump events of a similar age from separate locations within a lake have been shown to be seismically triggered (Van Daele et al., 2015). While it is possible a non-seismically generated mass wasting event could form lacustrine slump deposits, Chapron et al. (1999), Schnellmann et al. (2002), and Moernaut et al. (2014) provide evidence to support ground shaking as a likely trigger. Schnellmann et al. (2002) interpreted slump deposits in the subsurface of Lake Lucerne, Switzerland as the result of earthquake events, while Moernaut et al., 2015 found slump deposits in Chilean lakes after large historic interplate earthquakes, including the 2010 M_w 8.8 and 1960 M_w 9.5 earthquake events. Additionally, the observed surface rupture to the north of the lake and offset beds within the lake indicate the region is seismically active and past earthquake events have occurred in the Lake Crescent area (Figs. 3 & 14). Therefore, the slump deposits in Lake Crescent are inferred to be seismically induced. Earthquake triggered movement of the sediments perched on a subaqueous slope could cause the previously emplaced lacustrine sediments to fold and deform. The event-free depth for the EL3 layers present in cores 1B-1K, 3C-1K, 4A-1K, and 8A-1K was calculated assuming a thickness of one half the total thickness of the event layer. The Bacon age model and accumulation rate for core 4A-1K were determined using an EL3 thickness of 38 cm (one half the total deposit thickness).

Three EL4 deposits, all from the northern basin, are present in piston cores 3C-1K, 7A-1K, 7C-1K, and 9A-1K. One additional EL4 layer was recorded in cores 1A-1K and 1B-1K, in the channel between the southern and northern basins. These deposits are >25 cm thick and composed of highly disturbed, mixed clay to coarse pebble-sized particles with organic matter (mainly twigs and woody

debris) interspersed throughout (Fig. 11). Cores 1A-1K, 1B-1K, 3C-1K and 9A-1K, all of which include EL4 deposits, were collected from locations where the bathymetry of the lake floor contains hummocky topography indicative of landslide deposits. These locations were also at the base of subaerial landslide scarps; therefore, this type of sedimentary deposit is inferred to be the result of a subaerial landslide transporting material directly into the lake. The steep slopes surrounding Lake Crescent are conducive to landslides which could conceivably be triggered by an earthquake. In cores 7A-1K, 7C-1K, and 9A-1K, landslide deposits 'grade' into the sandy basal layer of the overlying megaturbidite, indicating their shared genesis. The timing of these events is determined to be the same as the above event layer deposits as the landslide is inferred to have generated the lake wide seiche and consequent reworking of lake sediments that are preserved in the homogenous sub-unit of the EL1 megaturbidites. The thickness of the landslide deposit as well as the force of the lake tsunami moving predominately away from the landslide location may explain why the landslide deposits are present in the record instead of eroded by the megaturbidite emplacement process.

The presence of multiple slump and landslide deposits directly beneath a correlated, widely distributed megaturbidite layer indicates that these events most likely occurred concurrently. Synchronous mass transport events have been assigned a seismic origin in several paleoseismic studies across the globe (Jibson, 1996; Schnellman et al., 2002; Moernaut et al., 2014). Landslide deposits in core 3C-1K produced a 2-sigma calibrated radiocarbon date that overlaps with the age range of EL1-C. Additional slump and landslide deposits in core 8A-1K directly underlie EL1-C and it seems likely these deposits formed just prior to emplacement of the overlying EL1-C layer. This indicates more than one mass transport event may have occurred simultaneously prior to the formation of EL1-C. Synchronous triggering of landslides and slumps indicates a ground shaking event large enough to overcome the structural integrity of multiple slopes surrounding and within the lake. Landslide and slump deposits in cores 1A-1K and 1B-1K, representing the channel sediment record, are located near the top of the retrieved cores and directly underlie a thinner turbidite layer that may be the same unit as the thicker EL1-A megaturbidite (Fig. 7c). Megaturbidites tend to pond in the deepest portions of the lakebed and may have only left a thin layer on the shallow landslide deposits present in the channel between the two lake basins. It is probable that many additional

landslide and slump deposits were not recovered by the 14 retrieved sediment cores. The presence of additional small slides on the lake floor and slumps on the lake margins are visible in the multibeam bathymetry indicating that these types of events are common in the lake's history (Fig. 4). If multiple subaerial mass transport events were triggered by an earthquake event they could conceivably trigger a lake tsunami and subsequent seiche forming a megaturbidite deposit. Ground shaking has been shown to remobilize sediment into and within lakes all around the world, often generating subaerial-to-lacustrine landslides, sub-lake slumps, and thick megaturbidite deposits (e.g. Inouchi et al., 1996; Chapron et al., 1999; Fanetti et al., 2008; Hilbe & Anselmetti, 2014; Moernaut et al., 2014; Van Daele et al., 2015, among others). It is likely that this process has occurred in Lake Crescent as well.

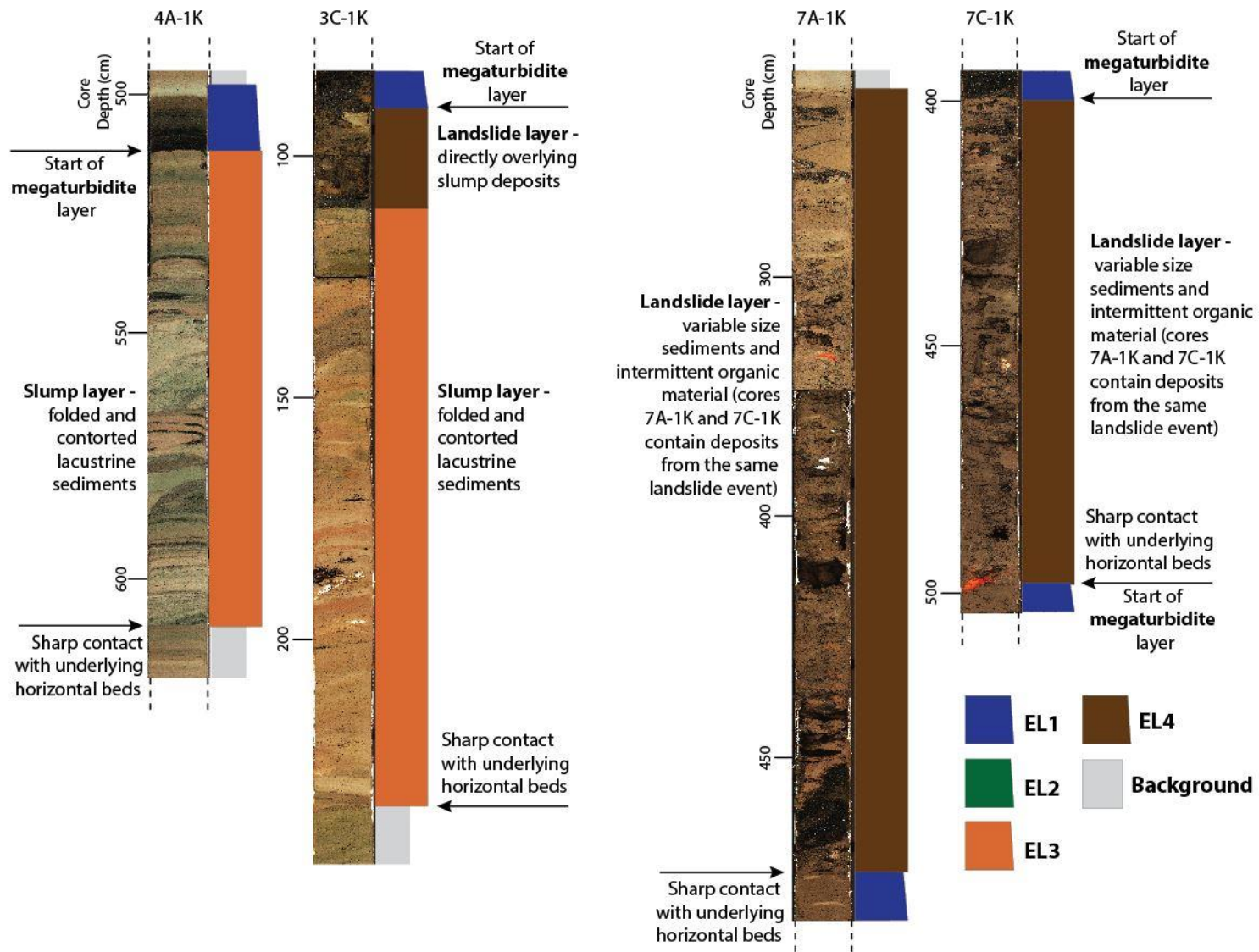


Figure 11. Core images and descriptions of landslide and slump deposits.

6. DISCUSSION AND INTERPRETATION

Megaturbidites, turbidites, slumps, and landslides present in Lake Crescent are inferred to represent ground shaking from seismic activity. These deposits indicate that at least four earthquakes large enough to trigger subaerial landslide events with a subsequent lake tsunami and seiche shook the Lake Crescent area in the past ~8,500 years while an additional 19 seismic events with smaller modified Mercalli intensity values may have occurred as recorded by “smaller” turbidites (Table 3). It is possible that this number is an overestimate as some of the 19 EL2 deposits could have formed from non-seismic triggers. However, this also may be an incomplete record as not every earthquake may have left a distinguishable sedimentary event layer. Moernaut et al. (2014) discuss an earthquake-recording threshold (EQRT) that corresponds to the specific seismic intensity that must be reached in order to trigger a turbidity current in a particular lake. The EQRT is primarily determined by the minimum seismic intensity needed to cause subaqueous mass failures in a lake, in turn dependent on slope angles, sedimentation rates, and sediment geotechnical properties, as well as the position of the coring location relative to failing slopes. The EQRT for several Chilean lakes was determined to be an earthquake with 5.5 moment-magnitude (M_w) (Moernaut et al., 2014).

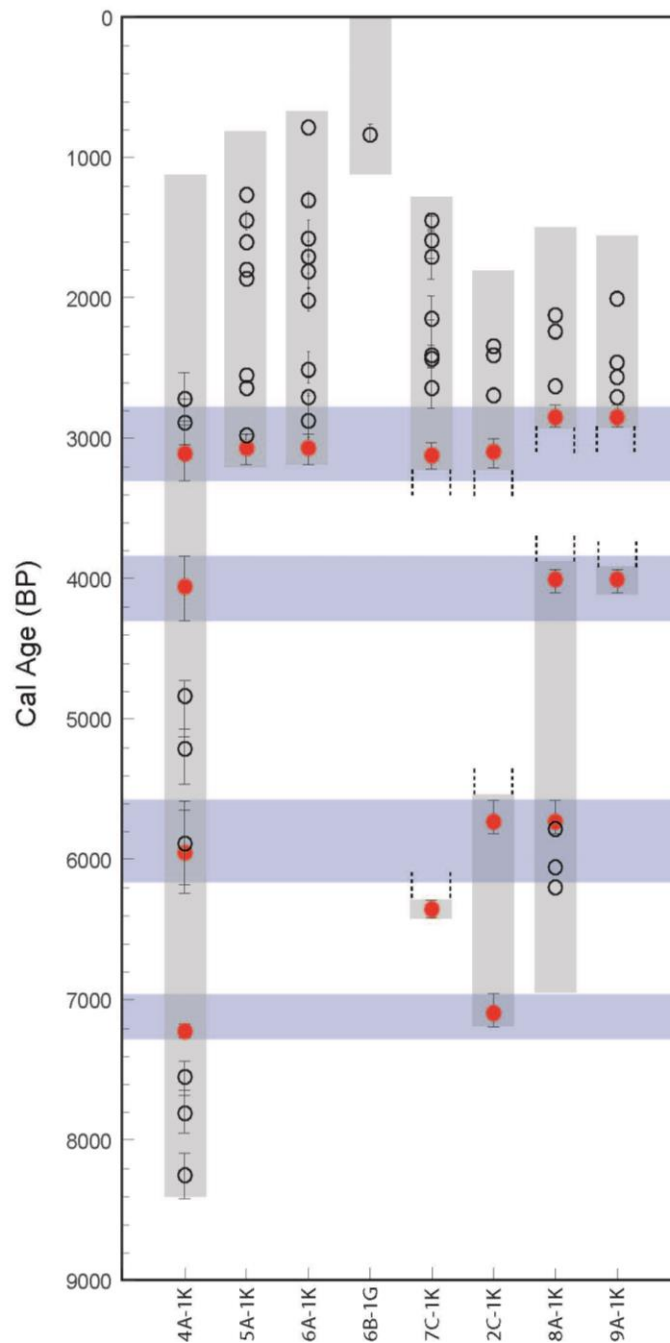


Figure 12. EL1 and EL2 event deposits correlated across Lake Crescent. Cores are organized in a transect starting in the far western depression in the elongate southern basin (Core 4A-1K) through the eastern portion of the smaller northern basin (9A-1K). Red circles represent megaturbidite deposits, while black outlines represent EL2 turbidite layers. Shaded blue areas represent the age range of each of the four widespread megaturbidite deposits in the sediment record while the gray areas indicate the total age range of each sediment core. Missing portions of the sediment record, most likely from the erosive emplacement of the megaturbidites, are indicated by dashed black lines. The amount of time missing from the top of each core was calculated using the 0.79 mm/yr average sediment accumulation rate (Appendix 5). The EL1-C deposit in core 7C-1K is correlated to the deposits in cores 4A-1K, 2C-1K, 8A-1K and therefore the anonymously old date of 6352 (6289-6411) cal BP was disregarded.

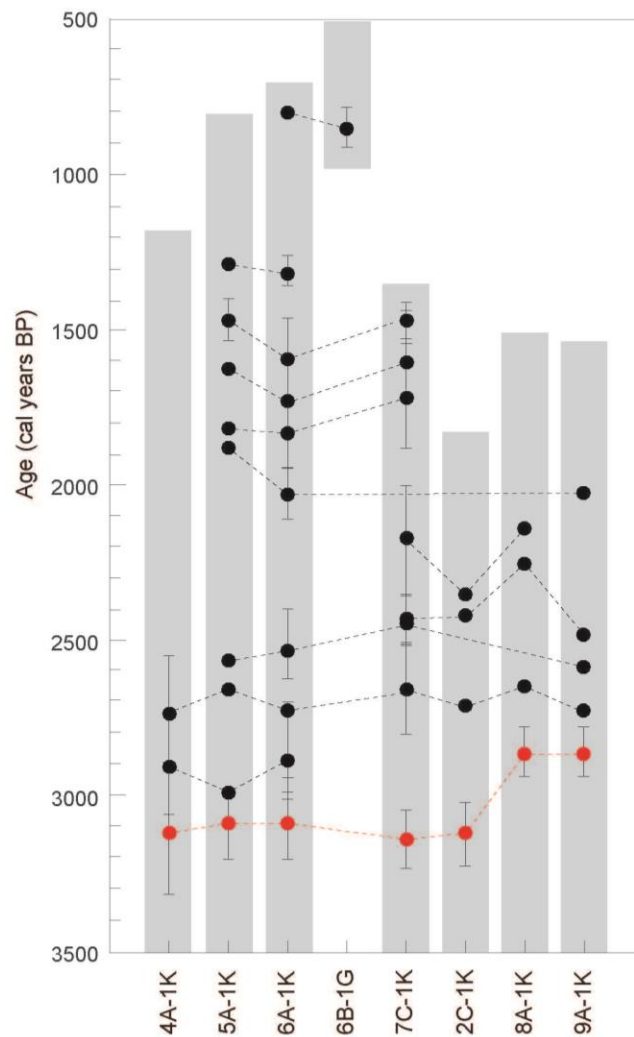


Figure 13. EL2 layers correlated (dashed black lines) above the first megaturbidite deposit (EL1-A) that is indicated by red symbology.

To further complicate matters, earthquakes can exacerbate the release of material from hillslopes and not only cause landslides into the lake, but also in the surrounding watershed. Earthquakes have been shown to increase sediment delivery to waterways by triggering landslides in tectonically active mountain belts (e.g., Dadson et al., 2004). Gullies on the steep slopes within the surrounding Lake Crescent watershed may give way and increase the amount of sediment available to be transported into the lake by episodic high precipitation events thereby producing a hyperpycnal flow. Therefore, a turbidite deemed to be triggered by a flooding event may also indicate that seismic activity occurred. The complexities associated with the different types of turbidites make it challenging

to definitively ascertain every earthquake induced deposit within Lake Crescent. Therefore, when correlating events across the lake only layers determined to be megaturbidites, or turbidites of significant thickness, were included (Figs. 12 & 13; Table 3).

There is strong evidence from numerous studies that the Cascadia subduction zone generates great earthquakes of magnitude 8.0 to 9.0+ (Atwater, 1987; Nelson et al., 2006, Goldfinger et al., 2012). A Shakemap scenario created by the U.S. Geological Society for a magnitude 9.0 earthquake occurring off the coast of southern Washington/Northern Oregon indicates the Lake Crescent region would experience subsequent ground shaking of modified Mercalli intensity VI-VII (USGS, 2016). These events would most likely exceed the EQRT at Lake Crescent and leave a sedimentary imprint in the lake stratigraphy. While offshore events may leave traces in the sedimentary record, local faults embedded in the upper crust of North America are also likely to trigger events affecting Lake Crescent. Significant evidence for a magnitude 7.0 to 7.5 event occurring 1100 cal yr BP on the nearby Seattle fault indicates that upper crustal faults could also have generated earthquakes that most likely exceeded the Lake Crescent EQRT (e.g., Atwater & Moore, 1992; Karlin et al., 2004). The topographic scarp visible on the Sadie Creek fault just north of Lake Crescent is evidence for past earthquakes that occurred along this fault that runs directly underneath the lake (Fig. 3). In addition to the surficial evidence of fault motion there is visible offset of sedimentary layers in the seismic data obtained from the northern basin (Fig. 14). The progressively offset sedimentary layers provide evidence for at least three seismic events that deformed the sediment under Lake Crescent in the past (Wegmann et al., 2014; Fig. 14). Nelson et al., 2007 found evidence for at least two and probably three earthquakes on the eastern segment of the Lake Creek-Boundary Creek fault some 10's of km to the east of Lake Crescent. These lines of evidence further support the idea that local faults left a significant sedimentary impact within the lake record. Lake Crescent most likely contains a record of both subduction zone and local and regional upper crustal earthquakes. Comparing the ages of event deposits present in Lake Crescent to other sedimentary records may help attribute these events to earthquakes that affected a broader region, possibly to ruptures along the subduction zone that extended over many 100's of km or to local faults that affected a smaller area.

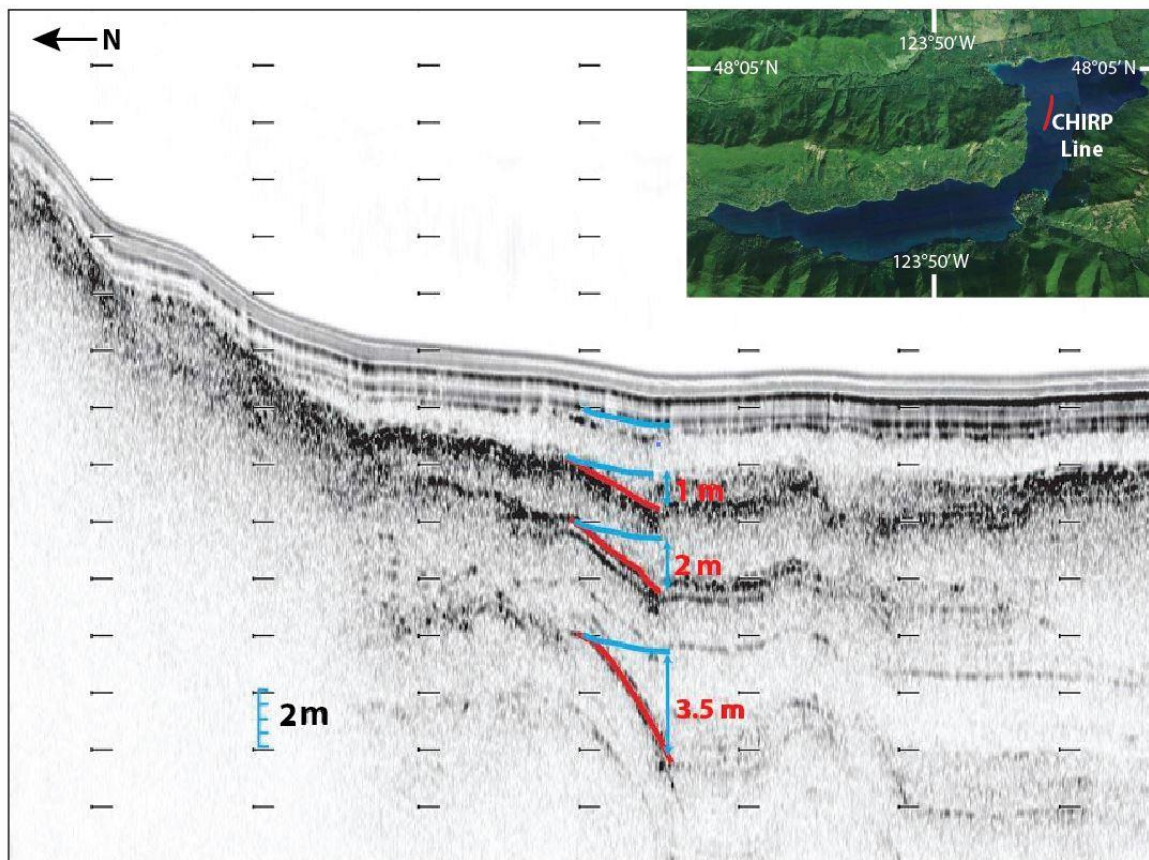


Figure 14. Offset sediment layers in a CHIRP seismic profile image. Progressive offset of the lake sediment layers indicates increasing fault motion underneath the lake. The uppermost lake sediments have not been deformed indicating they have not experienced the fault motion.

The timing of paleoseismic events from the Lake Crescent record is compared to earthquake records obtained using offshore turbidites, tsunami deposits, and surficial deformation from faulting documented in southwestern British Columbia and offshore western Washington (Table 4 & Fig. 15). The paleoseismic chronology from Effingham Inlet, a fjord located ~150 km northwest of Lake Crescent, on the Pacific coast of Vancouver Island, British Columbia, was determined using 'seismite' deposits identified by their composition of re-suspended, mixed, and re-deposited laminated sediments. These deposits were interpreted to represent mass-wasting events from the surrounding bedrock walls and/or from subaqueous delta failures during ground shaking events (Enkin et al., 2013). Radiocarbon dating of terrestrial plant debris indicates that the Effingham inlet seismites record earthquakes with an $\sim 550 \pm 400$ year recurrence interval (Enkin et al. 2013). Similarly, a

4,000-year earthquake record in Saanich Inlet, ~70 km northeast of Lake Crescent, on southeast Vancouver Island was inferred from massive, coarse layers interpreted as earthquake-triggered submarine debris flows (Blaise-Stevens et al., 2011). Based on varve counts, ^{137}Cs geochronology, a biohorizon marking 1940 CE, and one radiocarbon age, Blaise-Stevens et al. (2011) suggested an average return period of ~470 year for earthquakes affecting Saanich Inlet.

The third comparison record is from Holocene deep-sea turbidite deposits in the offshore Cascadia Basin. These turbidites have been used to infer a recurrence interval of ~500 to 530 yr for great earthquakes on the Cascadia Margin (Goldfinger et al., 2012). Multiple locations were sampled from offshore Vancouver Island to Cape Mendocino and turbidites were correlated and radiocarbon dated (Goldfinger et al., 2012). These authors conclude that synchronous turbidite deposits along the entire Cascadia margin can only be explained by shaking associated with a great earthquake. All the event layers included in Fig. 15 were correlated to offshore Vancouver Island ensuring that the northern portion of the Cascadia subduction zone ruptured and therefore associated ground shaking could have affected Lake Crescent.

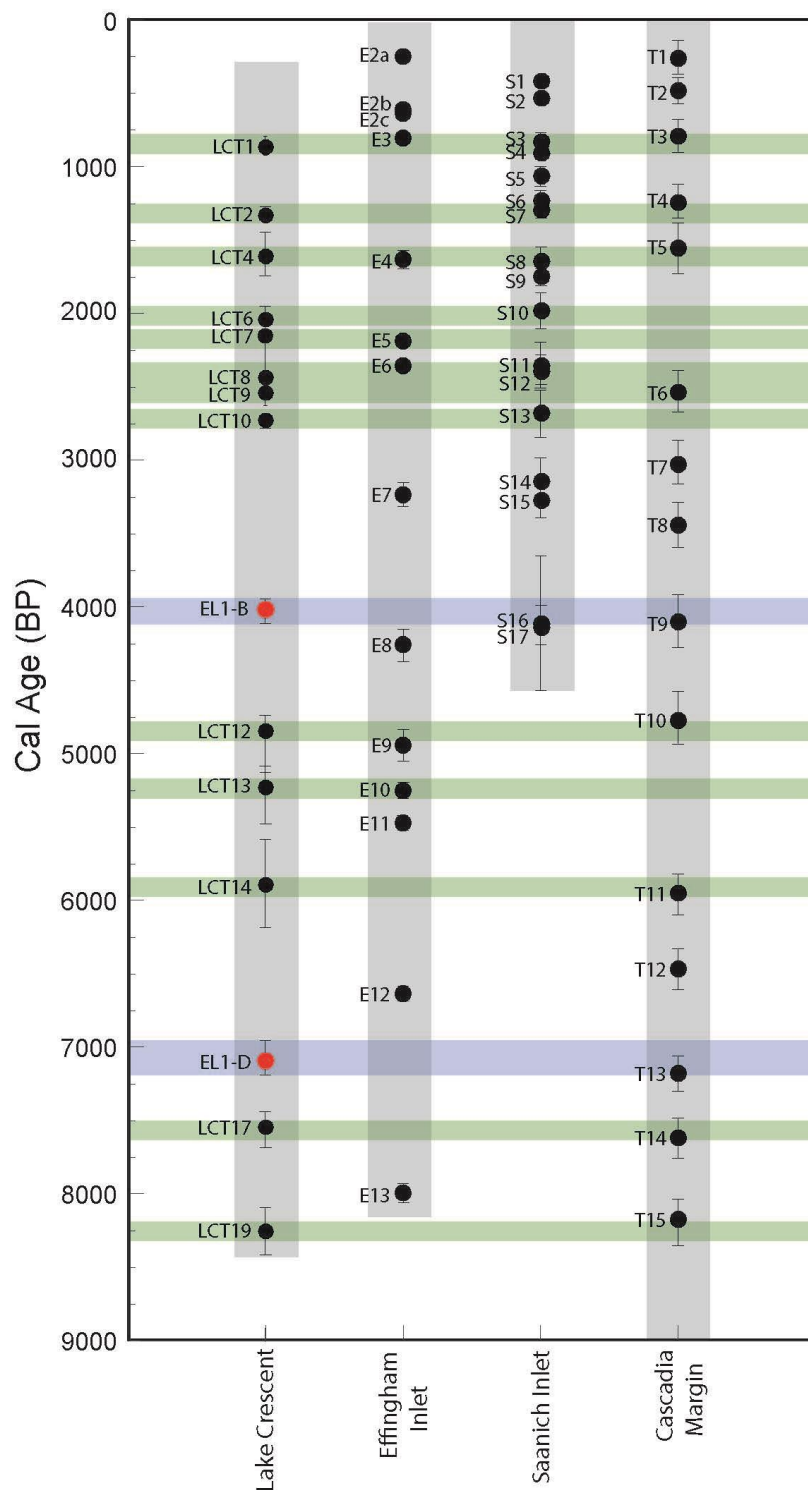


Figure 15. Age of Lake Crescent EL1 (solid red circles) and LCT (solid black circles) deposits compared to the seismic records of Effingham Inlet (Enkin et al., 2013), Saanich Inlet (Blaise-Stevens et al., 2011), and the combined offshore Cascadia margin turbidite record (Goldfinger et al., 2012). Blue shaded intervals show age range of megaturbidite deposits while green shaded intervals indicate the range of correlated Lake Crescent turbidites (EL2). Only EL2 layers that correlated to at least one additional record outside of Lake Crescent were included (Table 4).

Table 4. Lake Crescent EL1 and EL2 layers correlated to the seismic event records of Effingham Inlet (Enkin et al., 2013), Saanich Inlet (Blaise-Stevens et al., 2011), and the combined Cascadia margin offshore turbidite record (Goldfinger et al., 2012). The age of LCT7 was determined from interpolation of accumulation rates and therefore is considered an estimate.

Lake Crescent Event Layer ID/Age	Effingham Inlet Event Layer ID/Age	Saanich Inlet Event Layer ID/Age	Offshore Turbidites ID/Age
LCT1 861±65	E3 803±27	S3 827±60	T3 796±117
LCT2 1328±48		S7 1293±55	T4 1243±124
LCT4 1617±148 [†]	E4 1633±60	S8 1644±98	T5 1554±177
LCT6 2033±83		S10 1982±123	
LCT7 (2137)	E5 2188±30		
LCT8 2517±165	E6 2353±37	S11 2353±156	T6 2536±147
LCT10 2628±122		S13 2685±160	
EL1-B 4005±83		S16 4112±458	T9 4108±190
LCT12 4749±201 [†]	E9 4945±110		T10 4770±19
LCT13 5167±196 [†]	E10 5255±55		
LCT14 5888±292 [†]			T11 5959±141
EL1-D 7124±118			T13 7182±122
LCT17 7534±123 [†]			T14 7625±138
LCT19 8246±160 [†]	E13 8000±64		T15 8173±183

Fig. 15 and Table 4 demonstrate that the majority (13 of 19) of EL2 deposits in Lake Crescent can be correlated to event layers in one or more paleoseismic records previously attributed to rupture of the northern Cascadia subduction zone or regional earthquakes. However, only two of the four EL1 (megaturbidite) units fall into the age range of a comparison record: EL1-B, which correlates to event deposits in Saanich Inlet (S16) and the offshore turbidite record (T9), and EL1-D which overlaps the age range of an offshore turbidite (T13) (Blaise-Stevens et al., 2011; Goldfinger et al., 2012). Therefore, it is possible that these two megaturbidites may have been triggered by a great earthquake that ruptured at least the northern portion of the Cascadia margin. However, the lack of a correlating event for EL1-A and EL1-C in the offshore record indicates that these events are not

bound to the occurrence of a subduction zone earthquake. It seems more likely that the mechanism that formed the thick EL1 deposits was a large landslide event that could have been triggered by rupture of one of the faults that runs directly underneath the lake, resulting in significant local ground motion and disturbance. An additional possibility is that the two correlated EL1 deposits formed when a subduction zone earthquake triggered rupture along the crustal faults under and near Lake Crescent. Sherrod & Gomberg (2014) inferred that great earthquakes of magnitude >8.6 have a high probability of triggering magnitude >6.5 upper crustal earthquakes in the greater Puget Sound region. The four EL1 events are separated by ~ 1000 - 3000 year long intervals. The last megaturbidite event dates to 2859 (2785-2943) cal yr BP indicating this type of event has not occurred for at least 2,851 years relative to the year 2016 CE.

Two identified LCT layers, LCT1 and LCT4, overlap with the age range of events identified in all three of the comparison paleoseismic records, while LCT2, LCT8, LCT12, and LCT19 correlate to two of the outside records (Table 4). The six LCT deposits in Lake Crescent that do not correlate to the comparison records may represent local faulting events affecting just the study area. Additionally, the Saanich Inlet record only includes events from the past $\sim 4,000$ years and therefore older events from this location were not able to be compared to the Lake Crescent events. An earthquake recurrence interval of ~ 320 years results if all 19 of the LCT events were seismically triggered. It is important to note this is a recurrence interval for all turbidite forming events and may represent ruptures occurring on different faults; therefore it is simply an estimate of the average time between ground shaking events experience at Lake Crescent on the northern Olympic Peninsula. However, the possibility that at least some of the EL2 deposits were formed from non-earthquake causes such as episodic floods cannot be discounted; therefore 320 years is likely a minimum recurrence interval.

Comparison of event layers present in the Lake Crescent sedimentary record supports the idea that the north Olympic Peninsula is affected by earthquakes rupturing local, upper-crustal faults, regional faults, and the northern portion of the Cascadia subduction zone. Eight of the LCT layers temporally overlapped with Cascadia margin offshore events; therefore, it seems likely that subduction zone earthquake events leave a sedimentary imprint in Lake Crescent. The remaining LCT deposits could have been triggered by smaller local earthquake events or regional fault ruptures.

The expected ground shaking intensity of VI-VII at Lake Crescent after a M_w 9.0 subduction event may leave a similar LCT deposit as a regional upper-crustal fault or a small local fault rupture occurring underneath the lake (USGS, 2016). Due to the many types of seismic events that could form LCT deposits it is not possible to precisely determine their origin without further analysis.

The 2 to 3 m fault scarp visible along the Sadie Creek fault in the LiDAR data indicates that earthquakes occurring on faults running directly underneath the lake have broken the ground surface in the past; this would conceivably leave a significantly large impact, such as a megaturbidite layer in the sediment record (Fig. 3). Several landslide scarps are visible on the slopes surrounding the lake including the large landslide deposit that separated Lake Sutherland and Lake Crescent. This landslide deposit, which has a maximum age of ~4340 cal yr BP, lies along the Sadie Creek fault and it seems likely that an earthquake occurring on this fault triggered the landslide event forming the ~4015 cal yr BP megaturbidite event layer (Wegmann et al., 2014).

Future work investigating the paleoseismic record of Lake Crescent should include additional attempts to sample the upper decimeters of the lake bed using methods such as freeze-cores since sediment from directly beneath the lake bed were generally not successfully sampled in either piston or gravity cores collected during this study. Additionally, dating of onshore landslides deposits and their correlation to the megaturbidite and turbidite layers within the lake might help to elucidate the mechanisms that led to their formation. Identifying sources of allochthonous sediment present in the event layers may help solidify their origins as well. This could be accomplished by sampling sediment obtained from the different tributaries that enter into the lake.

7. CONCLUSIONS

7.1 Summary

The sedimentary archive of Lake Crescent records 23 separate events inferred to be from earthquakes that occurred in the past ~8500 years. This could be a maximum estimate if some of the deposits were non-seismically triggered or a minimum estimate if layers were erased by scour from younger events. It is likely both scenarios have occurred. Megaturbidite and landslide deposits present in the lake sediment record indicate that earthquake triggered landslides generated

catastrophic lake tsunami and subsequent seiches at least four times in the past ~8500 years. Smaller turbidites most likely provide a sedimentary imprint of earthquakes as well, but difficulties in determining their method of origin complicates causative interpretations. Correlation of turbidite deposits through both basins as well as the large amount of sediment transported at one time to form a single turbidite layer provides evidence that these deposits were seismically induced. The 15 correlated event deposits between the Lake Crescent record and the seismic chronologies from three separate sites further suggest that Lake Crescent preserves a record of earthquakes. Distinct sedimentary event layers in the Lake Crescent record provide strong evidence that the region has experienced large seismic events in the past, elucidating the risk that these types of events are very likely to happen in the future.

7.2 Seismic Hazards

The presence of thick, rapidly deposited event layers in the sediment record of Lake Crescent indicates that landslides and subaqueous slumps on the margins of Lake Crescent present a significant geologic hazard. Historical records from Lake Lucerne, Switzerland report that a lake tsunami with a run-up of greater than 5 m occurred after a nearby earthquake shook the ground triggering sublacustrine mass transport events in 1601 A.D. (Hilbe & Anselmetti, 2014). If a subaerial slope failure transported material into the lake at rapid speed (>80 kmh) the displacement waves could reach 50 to 100 meters in size (Clark et al., 2015). A tsunami of this magnitude would be devastating to those living along the shore or visiting Lake Crescent. The last event large enough to generate a megaturbidite deposit was ~2850 years ago; the presence of additional megaturbidite deposits within the sedimentary record indicate that this type of event has occurred at least four times in the past c. 8500 years, therefore the lake may be overdue for a large catastrophic event. The upper part of the sedimentary record (i.e., the past 500 years), was not recovered in this study and it is unclear when the last seismic event that impacted the lake occurred. Therefore, additional sampling that records the uppermost lake sediment is paramount to identifying the risk associated with the turbidite events. Regardless, it is clear that Lake Crescent has experienced catastrophic earthquakes, lake tsunamis, and lake seiches in the past and most likely will again in the future.

REFERENCES

- Adams, J. (1990) Paleoseismicity of the Cascadia subduction zone: Evidence from turbidites off the Oregon-Washington margin. *Tectonics* v. 9(4), p. 569-583.
- Atwater BF. (1987) Evidence for great Holocene earthquakes along the outer coast of Washington state. *Science* v. 236, p. 942-944.
- Atwater, B.F., Hemphill-Haley, E. (1997) Recurrence intervals for great earthquakes of the past 3,500 years at northeastern Willapa Bay, Washington. *U.S. Geological Survey Professional Paper 1576*, 108 p.
- Atwater, B.F., Moore, A.L. (1992) A tsunami about 1000 years ago in Puget Sound, Washington. *Science* v. 258(5088), p. 1614-1617.
- Atwater, B.F., Yamaguchi, D.K. (1991) Sudden, probably coseismic submergence of Holocene trees and grass in coastal Washington State. *Geology* v. 19, p. 706-709.
- Babcock, R.S., Suczek, C.A., Engebretson, D.C. (1994) The crescent "terrane", Olympic Peninsula and southern Vancouver Island. *Washington Division of Geology and Earth Resources Bulletin* v. 80, p. 141-157.
- Beck, C. (2009) "Late Quaternary lacustrine paleo-seismic archives in north-western Alps: Examples of earthquake-origin assessment of sedimentary disturbances. *Earth-Science Reviews* v. 96, p. 327-344.
- Bertrand, S., Charlet, F., Chapron, E., Fagela, N., De Batist, M. (2008) Reconstruction of the Holocene seismotectonic activity of the southern Andes from seismites recorded in Lago Icalma, Chile, 39°S. *Palaeogeography Palaeoclimatology Palaeoecology* v. 259(2-3), p. 301-322.
- Blaauw, M. and Christen, J.A. (2011) Flexible paleoclimate age-depth models using an autoregressive gamma process. *Bayesian Analysis* v. 6, p. 457-474.
- Blais-Stevens, A., Rogers, G.C., Clague, J.J. (2011) A revised earthquake chronology for the last 4,000 years inferred from varve-bounded debris-flow deposits beneath an inlet near Victoria, British Columbia. *Bulletin of the Seismological Society of America* v. 101(1), p. 1-12.

- Chapron, E., Beck, C., Pourchet, M., Deconinck, J.F. (1999) 1822 earthquake-triggered homogenite in Lake Le Bourget (NW Alps). *Terra Nova* v. 11, p. 86-92.
- Clague, J.J. (1997) Evidence for large earthquakes at the Cascadia subduction zone. *Reviews of Geophysics* v. 35(4), p. 439-460.
- Clark, K.J., Upton, P., Carey, J., Rosser, B., Strong, D. (2015) Tsunami and Seiche Hazard Scoping Study for Lakes Tekapo, Pukaki, Ohau, Alexandrina and Ruataniwha, *GNS Science Consultancy Report 2014/227*. 82 p.
- Conze, R., Krysiak, F., Reed, J., Chen, Y., Wallrabe-Adams, H., Graham, C. and the New Jersey Shallow Shelf Science Team, Wennrich, V. and the Lake El'gygytgyn Science Team. (2010) New integrated data analyses software components. *Scientific Drilling* v. 9, p. 30-31.
- Cysat, R. (1601). *Collectanea Chronica und denkwürdige Sachen pro Chronica Lucernensi et Helvetiae*, in Schmid, J., *Quellen und Forschungen zur Kulturgeschichte von Luzern und der Innerschweiz*, Volume 1: Luzern, Diebold Schilling Verlag, p. 882-888.
- Dadson, S.J., Hovius, N., Chen, H., Dade, W.B., Lin, J.C., Hsu, M.L., Lin, C.W., Horng, M.J., Chen, T.C., Milliman, J., Stark, C.P. (2004) Earthquake-triggered increase in sediment delivery from an active mountain belt. *Geology* v. 32(8), p. 733-736.
- Enkin, R.J., Dallimore, A., Baker, J., Southon, J.R., Ivanochko, T. (2013) A new high-resolution radiocarbon bayesian age model of the Holocene and late Pleistocene from core MD02-2494 and others, Effingham inlet, British Columbia, Canada; with an application to the paleoseismic event chronology of the Cascadia subduction Zone. *Canadian Journal of Earth Sciences* v. 50, p. 746-760.
- Fanetti, D., Anselmetti, F.S., Chapron, E., Sturm, M., Vezzoli, L. (2008) Megaturbidite deposits in the Holocene basin fill of Lake Como (Southern Alps, Italy). *Palaeogeography Palaeoclimatology Palaeoecology* v. 259, p. 323-340.
- Gavin, D.G. (2001) Estimation of inbuilt age in radiocarbon ages of soil charcoal for fire history studies. *Radiocarbon* v. 43(1), p. 27-44.

- Gilli, A., Anselmetti, F.S., Glur, L., Wirth, S.B. (2013) Lake sediments as archives of recurrence rates and intensities of past flood events. In: Dating torrential processes on fans and cones, Methods and their application for hazard and risk assessment. Series Volume 47 ed. *Springer Science+Business Media Dordrecht: Springer Netherlands*. p. 225-242.
- Goldfinger, C., Nelson, C.H., Morey, A.E., Johnson, J.E., Patton, J.R., Karabanov, E., Gutiérrez-Pastor, J., Eriksson, A.T., Gràcia, E., Dunhill, G., Enkin, R.J., Dallimore, A., Vallier, T. (2012) Turbidite Event History—Methods and Implications for Holocene Paleoseismicity of the Cascadia Subduction Zone. *U.S. Geological Survey Professional Paper 1661–F* p. 332.
- Hallet, D.J., Hills, L.V., Clague, J.J. (1997) New accelerator mass spectrometry radiocarbon ages for the Mazama tephra layer from Kootenay National Park, British Columbia, Canada. *Canadian Journal of Earth Science* v. 34, p. 1202-1209.
- Heaton, T.H., Hartzell, S.H. (1987) Earthquake hazards on the Cascadia subduction zone. *Science* v. 236(4798), p. 162-168.
- Hilbe, M., Anselmetti, F.S. (2014) Signatures of slope failures and river-delta collapses in a perialpine lake (Lake Lucerne, Switzerland). *Sedimentology* v. 61, p. 1883-1907.
- Hutchinson, I., McMillan, A.D. (1997) Archaeological evidence for village abandonment associated with late Holocene earthquakes at the northern Cascadia subduction zone. *Quaternary Research* v. 48, p. 79-87.
- Inouchi, Y., Kinugasa, Y., Kumon, F., Nakano, S., Yasumatsu, S., Shiki, T. (1996) Turbidites as records of intense palaeoearthquakes in Lake Biwa, Japan. *Sedimentary Geology* v. 104(1–4), p. 117-125.
- Jensen, F.B., Kuperman, W.A., Michael, M.B., and Schmidt, H., (2011) *Computational Ocean Acoustics, Second Edition*, Springer, New York, p 794.
- Jibson, R.W. (1996) Use of landslides for paleoseismic analysis. *Engineering Geology* v. 43 (4), p. 291–323.

- Karlin, R.E., Abella, S.E.B. (1992) Paleoearthquakes in the Puget Sound region recorded in sediments from Lake Washington, U.S.A. *Science* v. 258(5088), p. 1617-1620.
- Karlin, R.E., Holmes, M., Abella, S.E.B., Sylwester, R. (2004) Holocene landslides and a 3500-year record of Pacific Northwest earthquakes from sediments in Lake Washington. *GSA Bulletin* v. 116(1/2), p. 94-108.
- Kremer, K., Hilbe, M., Simpson, G., Decrouy, L., Wildi, W., Girardclos, S. (2015) Reconstructing 4000 years of mass movement and tsunami history in a deep peri-alpine lake (Lake Geneva, France-Switzerland). *Sedimentology* v. 62, p. 1305-1327.
- Puget Sound LiDAR Consortium. (2015) Northwestern Olympic Peninsula, WA: Terrapoint. Seattle, WA. <http://pugetsoundlidar.ess.washington.edu/index.htm>. LiDAR Bare Earth DEM, computer file, [April 11th, 2016].
- Logan, R.L., Schuster, R.L. (1991) Lakes divided: The origin of Lake Crescent and Lake Sutherland, Clallam County, Washington. *Washington Geology* v. 19, p. 38-42.
- Mazzotti, S., Dragert, H., Hyndman, R.D., Miller, M.M., Henton, J.A. (2002) GPS deformation in a region of high crustal seismicity: N. Cascadia forearc. *Earth and Planetary Science Letters* v. 192, p. 41-48.
- McCaffrey, R., Qamar, A.I., King, R.W., Wells, R.E., Ning, Z., Williams, C.A., Stevens, C.W., Volick, J.J., Swick, P.C. (2007) Fault locking, block rotation, and crustal deformation in the Pacific Northwest. *Geophysical Journal International* v. 169, p. 1315-1340.
- Meszaros, J. and Fiegenger, M. (2002). Effects of the 2001 Nisqually Earthquake on Small Businesses in Washington State. *Economic Development Administration, U.S. Department of Commerce*, 47 p.
- Milliman, J.D., Farnsworth, K.L. (2011) River discharge to the coastal ocean: A global synthesis. *Cambridge University Press*.
- Moernaut, J. and De Batist, M. (2011) Frontal emplacement and mobility of sublacustrine landslides: results from morphometric and seismostratigraphic analysis. *Marine Geology* v. 285, p. 29-45.

- Moernaut, J., Van Daele, M.V., Heirman, K., Fontijn, K., Strasser, M., Pino, M., Urrutia, R., De Batist, M. (2014) Lacustrine turbidites as a tool for quantitative earthquake reconstruction: New evidence for a variable rupture mode in south central Chile. *Journal of Geophysical Research Solid Earth* v. 119, p. 1607-1633.
- Moernaut, J., Van Daele, M., Strasser, M., Clare, M.A., Heirman, K., Viel, M., Cardenas, J., Kilian, R., Ladron de Guevara, B., Pino, M., Urrutia, R., De Batist, M. (2015) Lacustrine turbidites produced by surficial slope sediment remobilization: A mechanism for continuous and sensitive turbidite paleoseismic records. *Marine Geology*. doi:10.1016/j.margeo.2015.10.009
- Moran, P.W., Cox, S.E., Embrey, S.S., Huffman, R.L., Olsen, T.D., Fradkin, S.C. (2013) Sources and sinks of nitrogen and phosphorus in a deep, oligotrophic lake, Lake Crescent, *Olympic National Park, Washington: U.S. Geological Survey Report 5107*. p. 1-56.
- Mulder, T., Zaragosi, S., Razin, P., Grelaud, C., Lanfumey, V., Bavoil, F. (2009) A new conceptual model for the deposition process of homogenite: Application to a cretaceous megaturbidite of the western Pyrenees (Basque region, SW France). *Sedimentary Geology*, v. 222(3-4), p. 263-273.
- Nelson, A.R., Kelsey, H.M., Witter, R.C. 2006. Great earthquakes of variable magnitude at the Cascadia subduction zone. *Quaternary Research* v. 65, p. 354-365.
- Nelson, A.R., Personius, S.F., Buck, J., Bradley, L., Wells, R.E., Schermer, E.R. (2007) Field and laboratory data from an earthquake history study of scarps of the Lake Creek–Boundary Creek fault between the Elwha River and Siebert Creek, Clallam County, Washington. *U S Geological Survey Scientific Investigations Map 2961*, 2 Sheets.
- Olsson, I. (1986) Radiometric methods. In: Handbook of Holocene palaeoecology and palaeohydrology. Berglund B, editor. Chichester: *John Wiley & Sons*. p. 273-312.
- Polenz, M., Wegmann, K.W., Schasse, H.W. (2004) Geologic map of the Elwha and Angeles Point 7.5 minute quadrangles, Clallam County, Washington. *Washington Division of Geology and Earth Resources Open File Report 1:24,000* (Clallam County, Washington), 1 Sheet.

- Reimer, P., Bard, E., Bayliss, A., Beck, J., Blackwell, P., Bronk Ramsey, C., Buck, C., Cheng, H., Edwards, R., Friedrich, M., Grootes, P., Guilderson, T., Hafliðason, H., Hajdas, I., Hatté, C., Heaton, T., Hoffmann, D., Hogg, A., Hughen, K., Kaiser, K., Kromer, B., Manning, S., Niu, M., Reimer, R., Richards, D., Scott, E., Southon, J., Staff, R., Turney, C., Van Der Plicht, J. (2013) IntCal13 and Marine13 Radiocarbon Age Calibration Curves 0–50,000 Years cal BP. *Radiocarbon* v. 55(4), p. 1869-1887.
- Schasse, H.W. (2003) Geologic map of the Washington portion of the Port Angeles 1:100,000 quadrangle. *Washington Division of Geology and Earth Resources Open File Report*, 1 Sheet.
- Schnellmann, M., Anselmetti, F.S., Giardini, D., McKenzie, J.A. (2005) Mass movement-induced fold-and-thrust belt structures in unconsolidated sediments in Lake Lucerne (Switzerland). *Sedimentology* v. 52(2), p. 271-289.
- Schnellmann, M., Anselmetti, F.S., Giardini, D., McKenzie, J.A. (2006) 15,000 years of mass-movement history in Lake Lucerne: Implications for seismic and tsunami hazards. *Eclogae Geologicae Helveticae* v. 99, p. 409-428.
- Schnellmann, M., Anselmetti, F.S., Giardini, D., McKenzie, J.A., Ward, S.N. (2002) Prehistoric earthquake history revealed by lacustrine slump deposits. *Geology* v. 30(12), p. 1131-1134.
- Shennan, I., Long, A.J., Rutherford, M.M., Green, F.M., Innes, J.B., Lloyd, J.M., Zong, Y., Walker, K.J. (1996) Tidal marsh stratigraphy, sea-level change and large earthquakes: A 5000 year record in Washington, U.S.A. *Quaternary Science Reviews* v. 15(10), p. 1023-1059.
- Sherrod, B., Gomberg, J. (2014) Crustal earthquake triggering by pre-historic great earthquakes on subduction zone thrusts. *Journal of Geophysical Research: Solid Earth* v. 119(2), p. 1273-1294.
- Siegenthaler, C., Finger, W., Kelts, K., Wang, S. (1987) Earthquake and seiche deposits in Lake Lucerne, Switzerland. *Eclogae Geologicae Helveticae* v. 80, p. 241-260.
- Smith, S. (2016). Tectonic and Climatic Controls on Landscape Evolution in the Hangay Mountains, Mongolia and Olympic Mountains, USA. Raleigh, NC: North Carolina State University. p. 57-81.

- Stover, C.W., Coffman, J.L. (1993) Seismicity of the United States, 1568-1989 (revised). United States Government Printing Office, Washington: 1993: *U.S. Geological Survey Professional Paper. Report 1527*. p. 388.
- Tabor, R.W., and Cady, W.M. (1978) Geologic map of the Olympic Peninsula: U.S. Geological Survey Map I-994, 2 sheets, scale 1:125,000.
- ten Brink, U.S., Song, J., Bucknam, R.C. (2006) Rupture models for the A.D. 900–930 Seattle fault earthquake from uplifted shorelines. *Geology* v. 34(7), p. 585-588.
- USGS. (2001) Clallam County: Mount Muller, Lake Crescent, Lake Sutherland. 10 m DEM. <http://gis.ess.washington.edu/data/raster/tenmeter/byquad/index.html> [May 27th 2016]
- USGS. (2016) Shakemap Scenario: uscasc9.0_expanded_peak_se. Earthquake Hazards Program. M 9.0 (Cascadia). http://earthquake.usgs.gov/earthquakes/shakemap/global/shake/casc9.0_expanded_peak_se/ [May 25th, 2016]
- Van Daele, M., Moernaut, J., Doom, L., Boes, E., Fontijn, K., Heirman, K., Vandoorne, W., Hebbeln, D., Pino, M., Urrutia, R., et al. (2015) A comparison of the sedimentary records of the 1960 and 2010 great Chilean earthquakes in 17 lakes: Implications for quantitative lacustrine palaeoseismology. *Sedimentology* v. 62, p. 1466-1496.
- Wegmann, K.W., Bohnenstiehl, D.R., Leithold, E.L., and Pringle, P.T. (2014) Earthquakes, mass wasting, and fish from northern Cascadia: Post-glacial rupture of the lake Creek-Boundary Creek fault revealed by Chirp seismic investigations at Lake Crescent, Washington: *Geological Society of America Abstracts with Programs*, v. 46, p. 779.
- Wells, R.E., Weaver, C.S., Blakely, R.J. (1998) Fore-arc migration in Cascadia and its neotectonic significance. *Geology* v. 26(8), p. 759-762.
- Yamaguchi, K.D., Atwater, B.F., Bunker, D.E., Benson, B.E., Reid, M.S. (1997) Tree-ring dating the 1700 Cascadia earthquake. *Nature* v. 389, p. 922-923.

APPENDICES

APPENDIX A. Major tributaries in the Lake Crescent watershed (Moran, 2013)

Tributary Name	Drainage Area (km²)
Barnes Creek	40.66
Fairholm Creek †	9.86
Un-named Tributary east of Lapoel Point	4.64
Smith Creek	3.56
Lapoel Creek	2.98
Cross Creek	2.38
Lake Crescent Tributary near Piedmont*	2.04
Aurora Creek	1.49
Eagle Creek †	1.48
Piedmont Creek*	1.37
Total Drainage Area	=70.46

*Piedmont Creek and the Lake Crescent Tributary near Piedmont are the only tributaries flowing into the Northern Basin.

†Fairholm Creek and Eagle Creek flow into the shallow depression in the western edge of the southern basin.

APPENDIX B. Accumulation rate calculations for sediment cores with multiple radiocarbon ages

Core ID	Median Age Range cal BP	2 σ cal Age Range BP	Event Free Thickness (cm)	Accumulation Rate
4A-1K	8505 – 2087	(8428-8587) - (1999-2285)	463 [†]	0.72 (0.70-0.75) mm/yr
5A-1K	3081 – 1470	(2963-3179) - (1407-1541)	106	0.66 (0.60-0.75) mm/yr
6A-1K	3081– 1318	(2963-3179) - (1280-1375)	147	0.83 (0.77-0.93) mm/yr
7C-1K	3133– 1468	(3037-3226) - (1393-1526)	132	0.79 (0.72-0.87) mm/yr

[†]Event free thickness for core 4A-1K was calculated using 0.5 of the EL3 deposit present in the sediment record.

APPENDIX C. Event layers present in the sediment record and their respective thicknesses and ages. Ages shown in red lettering were obtained through radiocarbon dating of organic material (Table 2). Ages bracketed by parentheses were interpolated using the accumulation rate calculated for that core and depth. Ages marked with † were interpolated using Bacon.

2C-1K Event Layer	2C-1K Layer Thickness	2C-1K Age	8A-1K Event Layer	8A-1K Layer Thickness	8A-1K Age	9A-1K Event Layer	9A-1K Layer Thickness	9A-1K Age
EL2-2C1	2 cm	(1897)	EL2-8A1	6 cm	(2137)	EL2-9A1	4 cm	(2023)
EL2-2C2	3 cm	(2100)	EL2-8A2	5 cm	(2251)	EL2-9A2	4 cm	(2251)
EL2-2C3	5 cm	(2351)	EL2-8A3	3 cm	(2643)	EL2-9A3	5 cm	(2479)
EL2-2C4	5 cm	(2416)	EL1-A	182 cm	2859 (2785-2943)	EL2-9A4	2 cm	(2580)
EL2-2C5	3 cm	(2707)	EL1-B?	16 cm	4015 (3921-4088)	EL2-9A5	6 cm	(2719)
EL1-A	150 cm	3112 (3003-3208)	EL1-C	152 cm	5736 (5656-5889)	EL1-A	28 cm	2859 (2785-2943)
EL1-C	193 cm	5736 (5656-5889)	EL3-8A1	122 cm	5736 (5656-5889)	EL1-B	23 cm	4015 (3921-4088)
EL2-2C6	4 cm	(6160)	EL4-8A1	55 cm	5736 (5656-5889)	EL4-9A1	>29 cm	4015 (3921-4088)
EL2-2C7	3 cm	(6413)	EL2-8A5	3 cm	(5786)	-	-	-
EL2-2C8	3 cm	(6666)	EL2-8A6	5 cm	(6052)	-	-	-
EL2-2C9	2 cm	(6729)	EL2-8A7	12 cm	(6204)	-	-	-
EL1-D	>52 cm	7097 (7006-7242)	EL2-8A8	7 cm	(6900)	-	-	-

4A-1K Event Layer	4A-1K Layer Thickness	4A-1K Age	5A-1K Event Layer	5A-1K Layer Thickness	5A-1K Age	6A-1K Event Layer	6A-1K Layer Thickness	6A-1K Age
EL2-4A1	5 cm	2732 [†] (2549-2918)	EL2-5A1	27 cm	(1288)	EL2-6A1	7 cm	(802)
EL2-4A2	6 cm	2904 [†] (2752-3080)	EL2-5A2	21 cm	1470 (1407-1541)	EL2-6A2	24 cm	1318 (1280-1375)
EL1-A	22 cm	3122 [†] (2925-3351)	EL2-5A3	21 cm	(1622)	EL2-6A3	21 cm	1591 [†] (1474-1721)
EL1-B	11 cm	4058 [†] (3821-4281)	EL2-5A4	33 cm	(1682)	EL2-6A4	17 cm	1727 [†] (1612-1846)
EL2-4A3	3 cm	4219 (4100-4402)	EL2-5A5	4 cm	(1818)	EL2-6A5	25 cm	1833 [†] (1722-1947)
EL2-4A4	7 cm	4839 [†] (4548-4949)	EL2-5A6	19 cm	(1879)	EL2-6A6	6 cm	1910 [†] (1803-2011)
EL2-4A5	3 cm	4851 [†] (4560-4959)	EL2-5A7	5 cm	(2485)	EL2-6A7	15 cm	2028 (1950-2115)
EL2-4A6	3 cm	N/A	EL2-5A8	8 cm	(2561)	EL2-6A8	6 cm	2493 [†] (2406-2623)
EL2-4A7	2 cm	4928 (4858-5037)	EL2-5A9	6 cm	(2652)	EL2-6A9	9 cm	2528 [†] (2436-2660)
EL2-4A8	4 cm	5220 [†] (4971-5362)	EL2-5A10	4 cm	(2985)	EL2-6A10	11 cm	2722 (2506-2750)
EL2-4A9	3 cm	5229 [†] (4983-5372)	EL1-A	173 cm	3081 (2963-3179)	EL2-6A11	6 cm	2884 [†] (2763-3060)
EL1-C	3 cm	5781 [†] (5500-6063)	-	-	-	EL1-A	157 cm	3081 (2963-3179)
EL2-4A10	3 cm	5888 [†] (5596-6181)	-	-	-	-	-	-
EL2-4A11	2 cm	6259 [†] (5940-6572)	-	-	-	-	-	-
EL1-D	13 cm	7218 (7167-7267)	-	-	-	-	-	-
EL2-4A12	4 cm	6962 [†] (6662-7210)	-	-	-	-	-	-
EL3-4A1	76 cm	6962 [†] (6662-7210)	-	-	-	-	-	-
EL2-4A13	2 cm	7417 [†] (7238-7569)	-	-	-	-	-	-
EL2-4A14	6 cm	7544 [†] (7411-7656)	-	-	-	-	-	-
Tephra	2 cm	7627 (7478-7620)	-	-	-	-	-	-
EL2-4A15	6 cm	7800 [†] (7655-7958)	-	-	-	-	-	-
EL2-4A16	9 cm	8247 [†] (8086-8406)	-	-	-	-	-	-

10A-1K Event Layer	10A-1K Layer Thickness	10A-1K Age	7A-1K Event Layer	7A-1K Layer Thickness	7A-1K Age	7C-1K Event Layer	7C-1K Layer Thickness	7C-1K Age	2A-1K Event Layer	2A-1K Layer Thickness	2A-1K Age
EL2-10A1	2 cm	N/A	EL2-7A1	2 cm	1468 (1393-1526)	EL2-7C1	3 cm	1468 (1393-1526)	EL2-2A1	3 cm	(1466)
-	-	-	EL2-7A2	2 cm	N/A	EL2-7C2	3 cm	N/A	EL2-2A2	6 cm	(2162)
-	-	-	EL2-7A3	3 cm	N/A	EL2-7C3	3 cm	N/A	EL2-2A3	4 cm	(2302)
-	-	-	EL2-7A4	3 cm	(1569)	EL2-7C4	4 cm	1601 [†] (1469-1765)	EL1-A	134 cm	2859 (2785-2943)
-	-	-	EL2-7A5	6 cm	(2199)	EL2-7C5	12 cm	1717 [†] (1554-1907)	EL1-C	182 cm	5986 (5921-6177)
-	-	-	EL2-7A6	3 cm	(2262)	EL2-7C6	6 cm	1846 [†] (1664-2041)	EL1-D	>24 cm	7097 (7006-7242)
-	-	-	EL2-7A7	3 cm	(2414)	EL2-7C7	5 cm	2165 [†] (1979-2331)	-	-	-
-	-	-	EL2-7A8	3 cm	2427 (2352-2681)	EL2-7C8	5 cm	2427 (2352-2681)	-	-	-
-	-	-	EL2-7A9	2 cm	(2707)	EL2-7C9	5 cm	2444 [†] (2378-2535)	-	-	-
-	-	-	EL2-7A10	2 cm	(2808)	EL2-7C10	8 cm	2645 [†] (2511-2795)	-	-	-
-	-	-	EL1-A	186 cm	2859 (2785-2943)	EL1-A	230 cm	3133 (3037-3226)	-	-	-
-	-	-	EL3-7A1	16 cm	2859 (2785-2943)	EL4-7C1	100 cm	3133 (3037-3226)	-	-	-
-	-	-	EL4-7A1	160 cm	2859 (2785-2943)	EL1-C	155 cm	6352 (6289-6411)	-	-	-
-	-	-	EL1-C	>198 cm	5736 (5656-5889)	-	-	-	-	-	-

1A-1K Event Layer	1A-1K Layer Thickness	1A-1K Age	1B-1K Event Layer	1B-1K Layer Thickness	1B-1K Age	3A-1K Event Layer	3A-1K Layer Thickness	3A-1K Age	3C-1K Event Layer	3C-1K Layer Thickness	3C-1K Age
EL2-1A1	6 cm	N/A	EL2-1B1	6 cm	N/A	EL2-3A1	16 cm	N/A	EL2-3C1	12 cm	N/A
EL4-1A1	87 cm	N/A	EL4-1B1	27 cm	N/A	EL1-A	2 cm	2859 (2785-2943)	EL1-C	68 cm	5736 (5656-5889)
-	-	-	EL3-1B1	182 cm	N/A	-	-	-	EL4-3C1	19 cm	5736 (5656-5889)
-	-	-	-	-	-	-	-	-	EL3-3C1	153 cm	5736 (5656-5889)

APPENDIX D. EL2 deposits volume and annual average sediment yield compared to the Hoh River (Milliman & Farnsworth, 2011)

Northern Basin annual amount of sediment discharge: $3.5 \text{ km}^2 * \frac{110 \text{ ton}}{\text{km}^2 \text{ yr}} = 385 \text{ ton/yr}$

Southern Basin annual amount of sediment discharge: $67 \text{ km}^2 * \frac{110 \text{ ton}}{\text{km}^2 \text{ yr}} = 7370 \text{ ton/yr}$

W. depression in the S. basin annual amount of sediment discharge: $11.5 \text{ km}^2 * \frac{110 \text{ ton}}{\text{km}^2 \text{ yr}} = 1265 \text{ ton/yr}^*$

*632.5 ton/yr was used for event layers in core 4A-1K to determine the number of years of average sediment yield represented

Northern Basin Volume Calculations

Layer Thickness	Thickness (km)	Area (km ²)	Volume (km ³)	Density* T/cm ³	Conversion	Tons	Years of avg. sediment yield represented
3 cm (min)	0.00003	3.472	1.04×10^{-4}	$\frac{2 \text{ tons}}{907185 \text{ cm}^3}$	$\frac{1 \times 10^{15} \text{ cm}^3}{1 \text{ km}^3}$	= 229,633 tons	≈ 596 yrs
4.5 cm (~average)	0.000045	3.472	1.56×10^{-4}	$\frac{2 \text{ tons}}{907185 \text{ cm}^3}$	$\frac{1 \times 10^{15} \text{ cm}^3}{1 \text{ km}^3}$	= 344,450 tons	≈ 895 yrs
12 cm (max)	0.00012	3.472	4.17×10^{-4}	$\frac{2 \text{ tons}}{907185 \text{ cm}^3}$	$\frac{1 \times 10^{15} \text{ cm}^3}{1 \text{ km}^3}$	= 918,534 tons	≈ 2386 yrs

*Density assumes 40% porosity: $2.0 \text{ gm/cm}^3 = (0.4)(1.0 \text{ g/cm}^3) + (0.6)(2.65 \text{ g/cm}^3)$

Southern Basin Volume Calculations

<i>Layer Thickness</i>	<i>Thickness (km)</i>	<i>Area (km²)</i>	<i>Volume (km³)</i>	<i>Density* T/cm³</i>	<i>Conversion</i>	<i>Tons</i>	<i>Years of avg. sediment yield represented</i>
4 cm (min)	0.00004	6.3943	2.56×10^{-4}	$\frac{2 \text{ tons}}{907185 \text{ cm}^3}$	$\frac{1 \times 10^{15} \text{ cm}^3}{1 \text{ km}^3}$	= 563,881 tons	≈ 77 yrs
14 cm (~average)	0.00014	6.3943	8.95×10^{-4}	$\frac{2 \text{ tons}}{907185 \text{ cm}^3}$	$\frac{1 \times 10^{15} \text{ cm}^3}{1 \text{ km}^3}$	= 1,973,582 tons	≈ 631 yrs
33 cm (max)	0.00033	6.3943	2.11×10^{-3}	$\frac{2 \text{ tons}}{907185 \text{ cm}^3}$	$\frac{1 \times 10^{15} \text{ cm}^3}{1 \text{ km}^3}$	= 4,652,015 tons	≈ 268 yrs

*Density assumes 40% porosity: $2.0 \text{ g/cm}^3 = (0.4)(1.0 \text{ g/cm}^3) + (0.6)(2.65 \text{ g/cm}^3)$

APPENDIX E. Amount of record missing from top of sediment cores calculations

Core ID	Age of Top of Core (BP)	Accumulation Rate (mm/yr)	Amount Missing
4A-1K	1229	0.72	79 cm
5A-1K	817	0.66	54 cm
6A-1K	638	0.83	59 cm
7C-1K	1342	0.79	106 cm
2C-1K	1801	0.79*	144 cm
8A-1K	1504	0.79*	119 cm
9A-1K	1542	0.79*	122 cm

*accumulation rate was assumed to be similar to the calculated rate from core 7C-1K